Astron. Astrophys. 141, 195–214 (1984)

ASTRONOMY AND ASTROPHYSICS

A high resolution hydrogen line survey of Messier 31

II. The warped flaring hydrogen layer

E. Brinks and W. B. Burton

Sterrewacht Leiden, Postbus 9513, 2300 RA Leiden, The Netherlands

Received May 25, accepted July 16, 1984

Summary. Some of the global aspects of the H I distribution in M31 are discussed on the basis of the high-resolution survey of the 21-cm line made with the Westerbork Synthesis Radio Telescope by Brinks and Shane (1984, Astron. Astrophys. Suppl. **55**, 179). The morphology of the H I kinematics and structure in M31 can be modelled by a flat disk extending over the region at $R < 16$ kpc, and, at larger radii, a flaring warped gas distribution. The scale height of the gas in the warped part of M31 increases approximately linearly with radius to a maximum scale height of about 1.7 kpc. The maximum deviation of the warp from the plane of the extended inner disk is about 3.8 kpc. These and other parameters of the warp in M31 are similar to those in our Galaxy. We have produced separate maps of the total surface brightness and of the velocity field of H I belonging to the warp and to the disk. The H I mass in the disk is about $2.4\ 10^9\ M_\odot$; the H I mass in the warp is about $1.5\ 10^9\ M_\odot$. As in our Galaxy, the flaring gas layer and the rather flat rotation curve in the regions of M31 require that the total mass there resides in a halo. The modelling procedure involves comparing synthetic line profiles with the observed situation and thus allows some judgements concerning the physical parameters of the gas; the same parameters of temperature, density, and velocity dispersion which roughly reproduce the H I spectra observed in our own Galaxy suffice also for M31. The 2π-symmetry and the general regularity of the warp in M31 argue against it being a consequence of interaction with the small elliptical companion M32. We further show that a well-defined integral-sign signature in the outer integrated intensity contours is not generally to be expected for a global warp of the sort seen in M31 and that the kinematic behaviour revealed by detailed H I surveys will in general prove a more useful tool for studying warps than integrated intensities.

Key words: galaxies: M31 – galaxies: kinematics and dynamics of – galaxies: structure of – radio lines: 21-cm

1. Introduction

Since the discovery of the warping of the layer of atomic hydrogen in our Galaxy (see e.g. Burke 1957; Kerr 1957; Westerhout 1957; Oort et al., 1958), increasing evidence has accumulated showing that for spiral galaxies large-scale and systematic deviations of the H I from a flat disk are common. Many of the edge-on galaxies studied by Sancisi (1976, 1983), including NGC 5907, NGC 4244, and NGC 4565, have a projected H I surface density which shows a characteristic integral-sign shape. For other galaxies like NGC 2841, NGC 5055, and NGC 7331 a warp is inferred on the basis of a twist of the kinematic line of nodes. Bosma (1981a, b) refers to this type of structure as a kinematical warp. Although most warps are apparently restricted to the gaseous component at large galactocentric radii, i.e. outside their Holmberg radii, some galaxies, of which NGC 4565 (van der Kruit and Searle, 1981a) is an example, also seem to possess a warp in the stellar distribution. Theoretical attempts to understand the formation and persistence of warps have been reviewed by Toomre (1983). The evidence on which these attempts are based remains sketchy in several respects. The overall form of the galactic potential is particularly puzzling. A more direct observational problem involves the kinematic and structural parameters of a warped system. The situation in our Galaxy is being clarified by new data (e.g. Henderson et al., 1982) and by new information on the outer-galaxy distance scale (e.g. Kulkarni et al., 1982). Knowledge of the detailed structural properties of warps in external galaxies requires the improved line-survey resolution which is now becoming available. In this paper we direct our attention to the warped gas layer in M31, analysing the new high resolution H I survey which was recently presented by Brinks and Shane (1984, Paper I of this series).

Since Baade (1963) pointed out a systematic deviation of Population II stars from the major axis at about 2° or 24 kpc distance from the nucleus, the warp of M31 has been the subject of various studies. In these studies there is considerable ambiguity in the use of the term warp. In the optical domain the warp discussed by Baade is easily confirmed on deep photographs. For example, Innanen et al. (1982) showed on deep red and yellow plates that the position angle defined by the outermost isophotes of the galaxy changes considerably with radius. Other discussions of warps or systematic deviations from equatorial symmetry in M31 refer to scales smaller than those of the entire outer-galaxy warp. For example, Arp (1964) pointed out a non-planer distortion of the distribution of H II regions, but this distortion occurs at much smaller radii than the H I warp which we consider here. In addition, it is restricted to the southern and south-eastern part of the disk. That this portion of the inner disk suffers from distortions is also apparent in the H I data of Brinks and Shane (1984) and in the IRAS infrared data discussed by Habing et al. (1984). It is plausible that these distortions represent a much more local phenomenon than the outer-galaxy warp. The possibility that the companion galaxy M32 could have an effect on the main disk of M31 was suggested by Baade (1963) and by Arp (1964). The nature of such an interaction was investigated by Byrd (1977, 1978) who showed that the effects could be appreciable over a limited region of the disk.

Send offprint requests to: W. B. Burton

From 21-cm line surveys we have known for some time that the H I layer of M31 is not flat. Roberts (1966), Roberts and Whitehurst (1975), and Newton and Emerson (1977) showed that the H I layer bends, at large distances from the centre, away from the major axis as defined by the main body of M31 and in the same direction as the optical warp. These conclusions were based principally on integrated H I properties. The recent detailed H I surveys made by Cram et al. (1980), using the 100-m Effelsberg telescope, and by Bajaja and Shane (1982) and Unwin (1980a, b; 1983), based on synthesis observations, contain sufficient kinematic detail to throw new light on the warping of the H I layer in M31 by revealing the presence of multiple-peaked spectra across the disk of the galaxy. Whitehurst et al. (1978) in their preliminary analysis of the Effelsberg data invoked a combination of a thick and mildly warped disk to account for the observed profiles. Using the same data base and a somewhat similar technique, Sawa and Sofue (1982) tried to delineate the warp assuming that the gas layer is thin. Although the sense and magnitude of warping derived by Sawa and Sofue agrees reasonably with the results of Whitehurst, Roberts, and Cram they fail to reproduce the multiple peaks in the H I spectra. Shane (1978) had suggested that the multiple-peaked spectra result from seeing a warped ring projected onto the central region of M31. The model developed by Henderson (1979), based on a thin H I layer which is warped into and crossing the line-of-sight, confirmed the interpretation proposed by Shane. Henderson's model accounts qualitatively for the earlier single-dish H I oberservations, but it is less succesful in reproducing the more detailed results from Paper I.

In this paper we describe how an improved warped galaxy model can lead to simulated profiles which reproduce some of the more detailed structure. In Sect. 2 we briefly review the salient observational data. In Sect. 3 we describe the geometry of the proposed model and in Sects. 4 and 5 discuss the signature of the model in synthetic H I profiles and compare the modelled situation with the one observed. In Sect. 6 we describe the method used to distinguish between the H I emission from the warp and from the disk, resulting in separate total-surface-brightness maps and velocity fields for the warp and for the disk. In Sect. 7 we compare the warp in M31 with the one observed in our Galaxy and in other systems. In Sect. 8 we summarize our conclusions.

2. Observations

Our analysis is based on the new 21-cm line survey of M31 made by Brinks and Shane (1984) with the Westerbork Synthesis Radio Telescope (WSRT) in its 1.5 km configuration and with the digital line backend giving a resolution of $\Delta\alpha \times \Delta\delta \times \Delta V = 24'' \times 36'' \times 8.2\,\mathrm{km\,s^{-1}}$. Five fields were observed which, after combining, covered M31 except for the extreme northern and southern parts (corresponding to distances from the nucleus along the major axis larger than about 75′). The velocity coverage extended from -618 to $-16\,\mathrm{km\,s^{-1}}$ (heliocentric). In this paper positions in M31 are given in a rectangular coordinate system, centred on M31 and aligned with the major axis, using the same nomenclature as in Paper I. This system is equivalent to the one introduced by Baade and Arp (1964).

Our paper is primarily concerned with the global distribution and motion of H I in M31. To enhance the low-level emission we therefore decided to smooth the data to a resolution of $\Delta\alpha \times \Delta\delta \times \Delta V = 48'' \times 72'' \times 8.2\,\mathrm{km\,s^{-1}}$. This data set (corresponding to data set (c) in Paper I) consists of 147 channel maps, each containing data from as many as five overlapping fields. The maps are corrected for the primary beam of the WSRT, which means that the noise varies as a function of position and velocity in the map. The position-velocity maps made on the basis of the data set (c) are particularly useful for the analysis of the large-scale structure. These maps show the brightness temperature of H I as a function of position and velocity along cross-cuts made perpendicular or parallel to the major axis of M31. A complete set of such diagrams is given in Paper I as Figs. 7 and 8. The resolution for the position-velocity maps made perpendicular to the major axis is $54'' \times 8.2\,\mathrm{km\,s^{-1}}$; for those made parallel to the major axis it is $60'' \times 8.2\,\mathrm{km\,s^{-1}}$. These figures demonstrate that the distribution and kinematics of H I in M31 is far from simple. The position-velocity maps made parallel to the major axis are especially suited to show that along almost every line-of-sight through M31 two separate velocity systems are sampled. One velocity structure is the familiar one due to a disk in differential rotation. The other one, which appears as an almost straight line in each of the maps and which has a shallower velocity gradient than that expected from a differentially rotating disk, we will confirm is due to warping of the plane into the line-of-sight. The two velocity systems, which show up dramatically in this new survey, had been noted before by Bajaja in the H I observations of the central area of M31 made using the WSRT with the analogue receiver (see Shane, 1975; Bajaja and Shane, 1982). They had also been noted by Cram, Roberts, and Whitehurst (1980) in the Effelsberg survey, and by Unwin (1983) in the Cambridge Half Mile Telescope survey. The position-velocity maps made parallel to the minor axis (see Fig. 7 in Paper I) show the multiple-peaked nature of the spectra from another aspect and demonstrate the East-West asymmetry of the outermost regions of M31.

3. Geometry of the model

The principal characteristics of the M31 H I data for wich a model should account are: (i) the multiple-peaked line profiles extending over most of the observed region; (ii) the kinematic gradients of the structures defined by these profiles; (iii) the asymmetries in these structures with respect to the axes of M31; and (iv) the velocity-widths and intensities of these structures. The most relevant previous kinematical model of M31 is the one proposed by Henderson (1979), based on the tilted ring model developed for M83 by Rogstad et al. (1974) and consisting of a series of thin concentric rings, each ring 1 kpc wide, and individually tilted in order to mimic a warped disk. In the Henderson model the warp sets in near 15 kpc and is oriented such that the line of nodes of the tilted rings is more or less parallel to the major axis of M31, so that the near side of the galaxy bends into the direction of the observer, putting the outer parts of the galaxy more edge-on. Henderson's model qualitatively works well, especially regarding the crucial point i).

Our model starts out with the same basic geometry as Henderson's but incorporates a number of modifications which allow us to address the additional points listed above. Instead of assuming a thin disk, we allow for the finite, varying thickness of the H I layer in which the gas density varies smoothly. Perhaps the most important difference is that we make the comparisons with the observations via synthetic spectra. This approach takes into account the fact that, just as in our Galaxy, many of the features of the modelled (and observed) H I spectra are more directly consequences of the velocity field rather than of gas density or temperature. An additional advantage of this approach is that parameters such as gas temperature, density, and velocity dispersion become relevant and therefore some estimate may be made of the values of these quantities in M31.

The transformation from spatial coordinates to the observed velocity space is not always easy to visualize, even if the model is an extremely simple one. For example, the simplest possible model for our Galaxy – a flat disk uniformly filled with gas moving in circles and viewed from its equator – nevertheless results after this transformation in synthetic velocity-longitude maps with substantial structure. If the disk is tilted with respect to the viewing coordinates and given a finite thickness, then the synthetic profile structures appear all the more complicated. This latter situation was modelled by Burton and Liszt (1978) in an attempt to simulate some of the apparent pecularities in the distribution of gas in the inner few kpc of our Galaxy. The model discussed here is a modification of this earlier one. The rotating, tilted, thick disk was put at the distance of M31. The disk was additionally modified by allowing the outer portion of the disk to be warped and to have a thickness depending on radius.

Figure 1 should serve to verify that the model is straightforward in concept. It consists of a disk, inclined by an angle i to the plane of the sky and extending to a maximum radius R_d. The thickness of the disk is expressed by the scale height, $h(r)$, of the H I gas layer and is a function of radius. The warp starts at R_d and extends over a distance of R_w. The midplane of the gas layer makes an angle ω with the extended central disk, such that the height of the warp above the extended central disk increases linearly with radius. This angle varies sinusoidally as a function of azimuth, γ, measured in the plane of the central disk. The scale height of the H I in the warp is also specified by $h(r)$. Although the concept is straightforward, the calculation of synthetic spectra is complicated by the wide range of parameter values and velocity projections encountered along a single line-of-sight. This wide range is a consequence of the finite thickness which we allow and is the principal reason that our model does not use the concentric ring approach of Rogstad, Lockhart, and Wright (1974). It would, of course, be quite attractive if parameters could be determined separately for each annulus in a model of concentric, tilted rings. However, the current observations are not suited to adequately constrain a model separately fit to individual rings. To restrict the number of model parameters we have used a coherent model of the gas layer, rather than a model built up of rings.

We will test our model and choose the free parameters by comparing line profiles calculated from the model with those

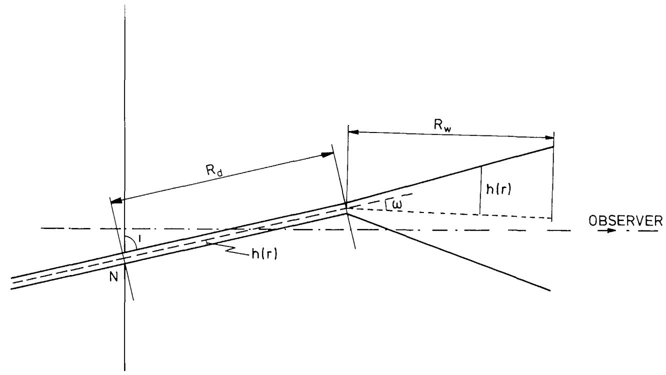

Fig. 1. Schematic representation of the geometry of the flaring warp model described in the test. The drawing shows the intersection of the plane through the observer and the minor axis of M31 with the nearer half of M31. The model is drawn to scale except that the thickness of the H I layer is three times the scale height

observed. We will calculate the profile in a direction specified by two coordinates, ξ and η, by integrating the contributions to the optical depth from intervals along this line-of-sight whose centres lie at distances d_p from the observer. The position of each such point, P, in M31 is described by cylindrical coordinates (r_d, γ, z_d) fixed with respect to the inner disk, where r_d is the perpendicular distance to the rotation axis, γ is an azimuthal angle measured in the sense of the rotation of M31 from the direction of the receding node to the direction of the point where P is perpendicularly projected onto the disk and z_d is the distance of P from the disk, positive on the side of the positive rotation axis. The directional coordinates, ξ and η, are very similar to (but not exactly the same as) the (X, Y) coordinates described in Paper I, where $\xi > 0$ corresponds to X north and $\eta > 0$ to Y east. The (X, Y) cartesian coordinates are defined by the properties of the Fourier transform and are described by Brouw (1975). ξ and η are spherical coordinates so defined that the equatorial plane, $\eta = 0$, coincides with the major axis of the image of M31, $Y = 0$, and ξ is measured from the direction toward the nucleus. The coordinate system is right-handed.

With the aid of these definitions, which are illustrated in Fig. 2a, the coordinates in M31 (r_d, γ, z_d), can be expressed in terms

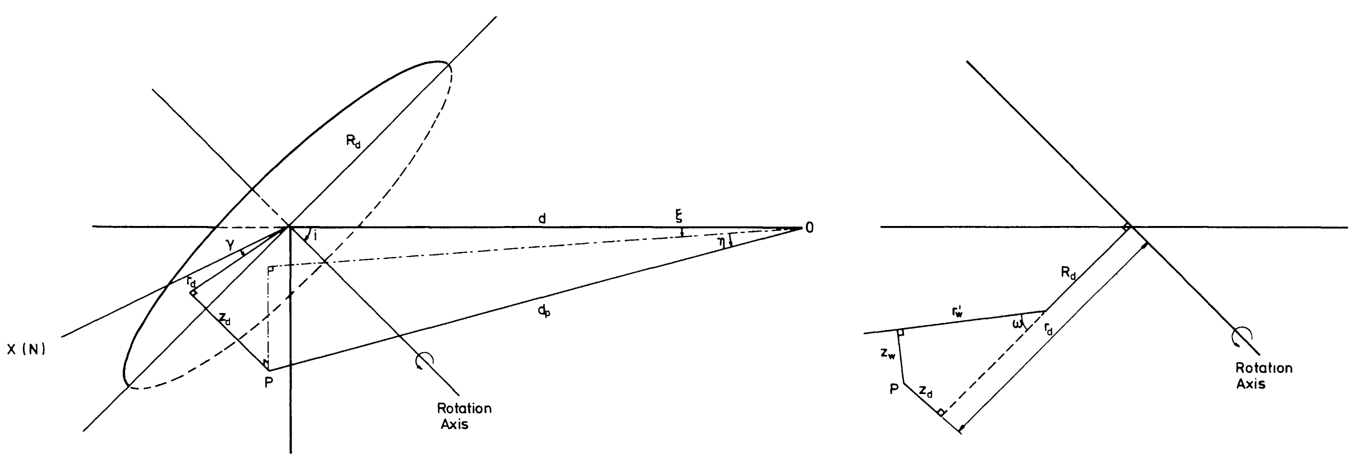

Fig. 2. **a** Schematic representation of the geometry of the model illustrating the coordinates of a point P, in the coordinate system defined in M31, (r_d, γ, z_d), and in the system defined with respect to the observer (ξ, η, d_p). **b** Schematic drawing showing the relevant geometry in the plane defined by the rotation axis of M31 and the point in question

of the coordinates with respect to the observer, (ξ, η, d_p). The distance, z_d, to the midplane of the disk is

$$z_d = d\cos i + d_p(\sin i \sin\eta - \cos i \cos\xi \cos\eta). \quad (1)$$

The perpendicular distance, r_d, from P to the rotation axis is

$$r_d = (d^2 + d_p^2 - 2dd_p \cos\xi \cos\eta - z_d^2)^{1/2}. \quad (2)$$

The azimuth, γ, is determined by

$$\sin\gamma = (d_p \cos\xi \cos\eta + z_d \cos i - d)/r_d \sin i, \quad (3a)$$

which in the case of a face-on galaxy reduces to

$$\sin\gamma = d_p \sin\eta / r_d. \quad (3b)$$

We assume throughout that the gas moves in circular orbits at velocities V_c which depend only on r_d, thus not on z_d. The observed radial velocity, V_p, at the point P is thus

$$V_p = V_s + V_c(r_d)\frac{d}{r_d}\sin i \sin\xi \cos\eta, \quad (4)$$

where V_s is the systemic velocity of the galaxy.

Figure 2b shows the geometry of the warped, outer part of the system, in the plane defined by the rotation axis of M31 and point P. The angle ω is constant along a given radius but varies sinusoidally as a function of azimuth according to

$$\omega(\gamma) = \omega_m \sin(\gamma + \gamma_0), \quad (5)$$

ω_m is the maximum angle which the warp makes with the extended inner disk and γ_0 indicates the angle which the line of nodes of the warp makes with respect to the line of nodes of M31. Using Fig. 2b we derive relationships applicable for a point in the warp analogous to those giving the cylindrical coordinates r_d, γ, and z_d, for a point in the disk. The perpendicular distance, z_w, from the point to the midplane of the warped layer is

$$z_w = (r_d - R_d)\sin\omega + z_d \cos\omega. \quad (6)$$

The distance from the onset of the warp to the projection of the point onto the midplane of the warp, r_w, is given by

$$r_w' = r_w - R_d = (r_d - R_d - z_w \sin\omega)/\cos\omega, \quad (7)$$

where r_w is the full distance from the nucleus to the projection of the point onto the warp as measured along the mean plane of the H I distribution.

Neither observations of H I at large radii in galaxies, nor theoretical models of warps present a clear picture of what to expect for the orientation of the velocity vectors in warped systems. In our model we assume that the H I gas in the warp moves in circular orbits parallel to the plane of the disk. The circular velocity depends only on radius, not on height above the plane. The orientation of the M31 warp is such that velocity vectors which are for example chosen parallel to the plane of the warp instead of parallel to the plane of the disk give results which are only marginally different over the part of the galaxy which we have observed. The radial velocity for an arbitrary point in the warped layer is thus

$$V_p = V_s + V_c(r_w)\frac{d}{r_d}\sin i \sin\xi \cos\eta. \quad (8)$$

In addition to the velocity field of the gas, one needs to describe its temperature, T_g, velocity dispersion, σ_g, and density. At $z=0$ the volume density is given by $n(r, 0)$. Which of the above distances are used for z and r depends on whether the point is located in the warped or unwarped part of the gas layer. Assuming a gaussian dependence on height above the plane, the volume density at any point is

$$n(r, z) = n(r, 0)\exp(-z^2/2h(r)^2), \quad (9)$$

where $h(r)$ is the scale height of the gas. Using the above formulae we can construct a model line profile, $\tau(V)$, giving the optical depth as a function of velocity for each line-of-sight. We calculated $\tau(V)$ at integral multiples of $2\,\mathrm{km\,s^{-1}}$ after dividing each line-of-sight into intervals Δl of 50 pc length (cf. Burton, 1971). Each interval contributes at velocity V

$$\Delta\tau_j(V) = 675.2\frac{n(r, z)\Delta l}{T_g \sigma_g}\exp\left(-\frac{1}{2}\left(\frac{V - V_j(r, z)}{\sigma_g}\right)^2\right). \quad (10)$$

The constant is evaluated for units of distances in kpc, velocities in $\mathrm{km\,s^{-1}}$, densities in atoms $\mathrm{cm^{-3}}$, and temperature in K. If a line-of-sight interval fell within the boundaries of the disk, i.e. $r < R_d$, formulae (1), (2), and (4) were used to find the values for z, r, and V_j; if it fell within the warped layer, formulae (6), (7), and (8) were used. The total optical depth is $\tau(V) = \Delta\tau_j(V)$, where the summation is over all intervals for which $|V - V_j(r, z)| < 3\sigma_g$. This optical-depth profile was converted to brightness temperatures to produce a synthetic spectrum

$$T_B(V) = T_g(1 - \exp(-\tau(V)). \quad (11)$$

The synthetic spectra were calculated on a ξ, η-grid with distances between grid points set at 0.6 arcmin, corresponding to the sampling interval in the observations, and resorted so as to simulate observations. We have not convolved the synthetic spectra with the WSRT beam because the structural and kinematic parameters of the model vary slowly on the scale of the beam.

4. Initial model of M31 based on a disk and a thin warp

4.1. Determination of the model parameters for the disk

The model described in the preceding section contains about a dozen parameters. The parameters were tested, and in some cases determined, by fitting the model to the observations. We adopt from other sources parameters to which the modelling is not particularly sensitive. Each parameter is discussed below, beginning with general parameters and those related to the disk component.

4.1.1. The distance, d, from the observer to the nucleus of M31

This distance was fixed at the familiar value of 690 kpc. Although recently values of 730 kpc (Kraan-Korteweg and Tammann, 1979) and 651 ± 53 kpc (de Vaucouleurs, 1978) have been suggested, retaining $d = 690$ kpc facilitates comparison with previous work.

4.1.2. The rotation curve, $V_c(r)$, and systemic velocity, V_s

Based on the WSRT survey and the work of Roberts et al. (1978) we adopt a rotation curve which consists of two linear segments, one rising from the nucleus representing a region of solid body rotation and the other representing a flat outer rotation curve. We find a value of $250 \pm 5\,\mathrm{km\,s^{-1}}$ (estimated error) for this flat part not corrected for inclination. This maximum velocity is reached at a radius of 5.2 kpc. The systemic velocity V_s is $-315 \pm 5\,\mathrm{km\,s^{-1}}$ (e.e.) if the rotation curves measured on the northern and southern

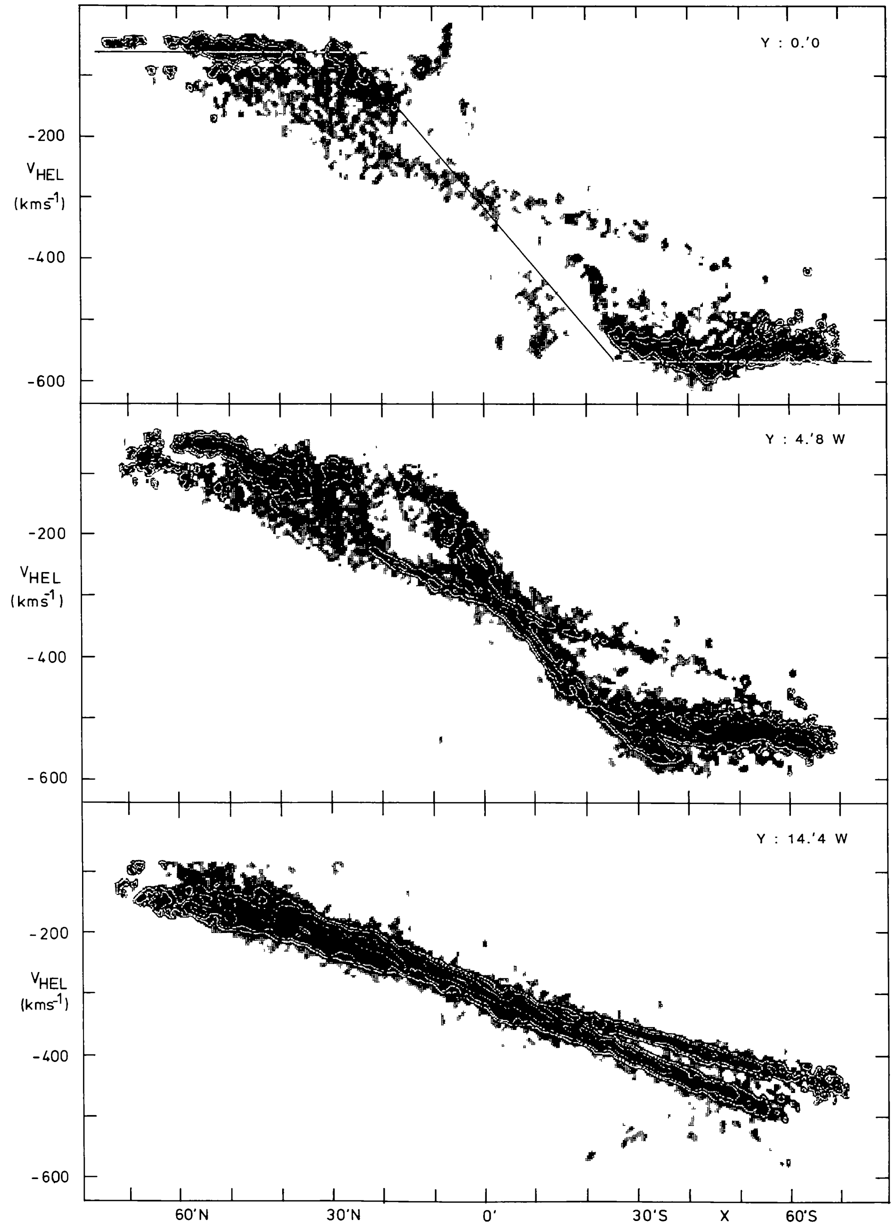

Fig. 3. Observed position-velocity maps made parallel to the major axis of M31. These maps, together with the orthogonal cuts in Fig. 5 and the more extensive material in Paper I, provide the principal observational constraints to the models. The grey-scale levels are 1.0, 1.5, 2.5, 5, 10, 25, and 50 K; the contour levels are 2.5, 5, 10, 25, and 50 K. The same contour and grey-scale levels are used for all observed and synthetic position-velocity maps

portions of the major axis are averaged. In Fig. 3 (top panel) we compare the adopted model curve with the observed major axis position-velocity map. We have ignored the wiggles in the envelope to the observed position-velocity distribution, which are of the order of 10–30 km s^{-1}. They may be related to deviations from circular motion in arm segments. A proper treatment of those wiggles requires detailed modelling similar to that in the study of M81 by Visser (1980a, b). The difficulty of identifying arm segments in M31 makes it poorly suited to such work, and in any case we prefer here a straightforward model of the global structure and kinematics. We similarly ignore the anomalous velocities in the inner 5 kpc (see e.g. Brinks, 1983). Because of the sensitivity of the modelled profiles to the input kinematics, an error of more than a few percent in the approximated rotation curve for the part of the disk exterior to the anomalous inner region would probably be detected. Our approximation of the observations at large radii by a flat rotation curve is given general justification by studies both in the optical domain (Rubin, Ford, and Thonnard, 1980; Rubin et al., 1982), and in the radio domain (e.g. Bosma, 1981b).

4.1.3. The inclination, *i*, of the disk

There have been various determinations of this angle. Arp (1964) gives an inclination which varies between 74° and 79°, based on a study of H II-regions, Pellet et al. (1978) find $i=77°30'$ based on their survey of emission-line regions. Henderson (1979) used $i=74°$ in his model derived from the H I observations of Cram et al. (1980). It is not clear, however, if he has taken resolution effects into account which would bring the inclination closer to 77°. We have checked the inclination angle by comparing the model position-velocity maps, in particular the maps parallel to the major axis, with the observed ones. An inclination of about 77° fits our observations better than one of about 74°, and because a value of 77° is more frequently encountered in the recent literature we have adopted this value.

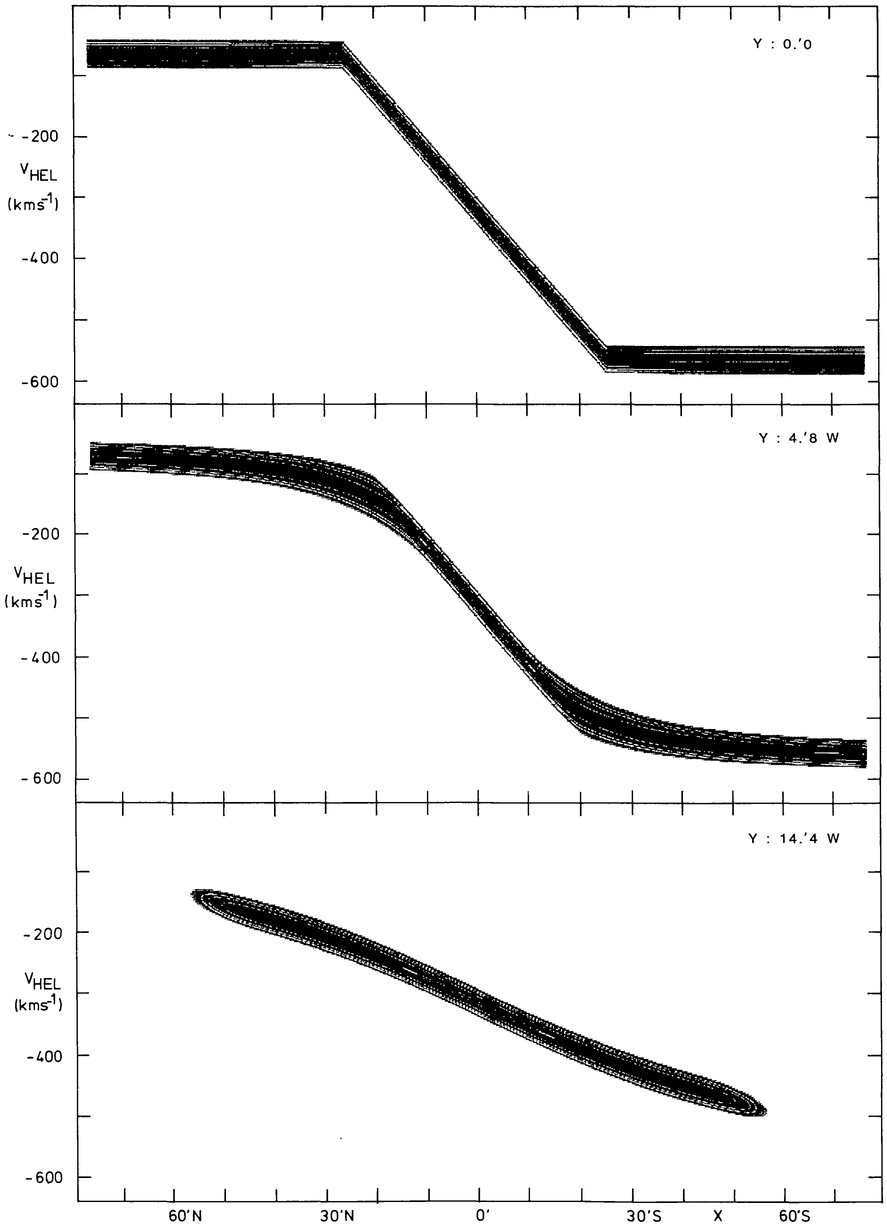

Fig. 4. Synthetic position-velocity maps produced from the initial flat-disk model described in the text and at the same positions as the observations shown in Fig. 3. The grey-scale and contour levels are the same as in Fig. 3

4.1.4. The radius, R_d, of the disk

The radius of the disk was determined by producing model position-velocity maps parallel to the major axis for disks of various sizes. These model calculations did not include any warping of the plane. The radius of the disk in the models was varied from 14.0 kpc to 18.0 kpc in 0.5 kpc intervals. The best fit was obtained for $R_d = 16.0$ kpc, with an estimated uncertainty of 0.5 kpc. The accuracy to which R_d can be determined depends on small scale deviations of the H I from a flat distribution and on the details of the H I distribution as a function of radius. Our value for R_d agrees with the radius at which the first tilted ring is encountered in Henderson's model.

4.1.5. The velocity dispersion, σ_g

Unwin (1983) found $\sigma_g = 8.1 \pm 0.9$ km s^{-1} for the H I gas in M 31. In determining this value Unwin accounted for beam-smearing and the presence of unseparated velocity components in the Cambridge spectra. Measurements of the dispersion in other galaxies show that it is roughly constant as a function of position in the galaxy. This is especially clear in the face-on galaxies NGC 3938 and NGC 628 observed by van der Kruit and Shostak (1982) and Shostak and van der Kruit (1984). Values for the velocity dispersion in these and other systems (see the discussion by van der Kruit 1981) range from 7 to 10 km s^{-1}. The value $\sigma_g = 8$ km s^{-1} which we adopt is consistent also with the situation in our Galaxy; the locally observed value is typically 5 km s^{-1}, but the clouds have a motion with respect to each other which would result in a higher estimate of the local value if the telescope beam covered as large an extent as in the case of external systems.

4.1.6. The scale height, $h(r)$, of the disk H I layer

For a constant σ_g the scale height of the H I layer increases with r. This scale height is inversely proportional to the mass volume density in the disk at $z=0$, $\varrho(r,o)$. Ignoring the mass contribution by the gas, the scale height of the gas is given by (see also Kellman, 1972)

$$h(r)=\sigma_g/[4\pi G\varrho(r,o)]^{1/2}. \quad (12)$$

If we use the mass model produced for M31 by Emerson (1976) and $\sigma_g=8\,\mathrm{km\,s^{-1}}$ we find for the expected scale height in the disk a value which ranges from about 60 pc at $r=5$ kpc to 185 pc at $r=15$ kpc. We note that in our Galaxy, however, the observed H I height remains approximately constant interior to the onset of the warp. To keep the number of free parameters limited and the model simple we decided to adopt a single value of 120 pc for the scale height of the gas in the disk. This value corresponds to the expected value for $r\simeq0$ kpc, where the main ring of H I emission is located, and is also the observed value of the H I scale height at that radius in our Galaxy.

4.1.7. The volume density, $n(r,z)$, of the disk H I layer

The volume density of the H I gas is described by Eq. (9). If we take the measured surface density of H I in the ring at about 10 kpc, which varies from 3.3 10^{20} at $\mathrm{cm^{-2}}$ to 6.6 10^{20} at $\mathrm{cm^{-2}}$ (Unwin 1980b), and if we use a scale height at that radius of 120 pc then the volume density at $z=0$ pc varies between 0.35 and 0.70 at $\mathrm{cm^{-3}}$. In most of our models we have set the volume density, $n(r,0)$, in the disk at a constant value of 0.60 at $\mathrm{cm^{-3}}$ (consistent with the situation in our Galaxy), but in the final stage of modelling some attempts were made to show the influence on the model spectra of the H I deficiency observed in the central 5 kpc and of the presence of arm-like segments.

4.1.8. The gas temperature, T_g

We know from various observations in our Galaxy that the temperature of the gas varies enormously in response to local circumstances. Nevertheless the global H I intensity structure can be modelled with a constant value of T_g ranging from 120 to 135 K. Presumably this represents some sort of mean, and in view of the comparable volumes sampled by the telescope beam in M31, it seems reasonable to adopt a single temperature, $T_g=125$ K.

4.2. Model for the disk of M31

Figures 3 and 5 show a selection of representative observed position-velocity maps parallel and perpendicular to the major axis, to which we compare our models using the same scales and intensity levels. Figure 4 (top panel) shows the model position-velocity map along the major axis made using the above parameter values. Comparing the model with the observations leads to the following remarks. Missing in this preliminary model is the H I running diagonally across the observed map contributed by the warped portion of M31 (see below). Almost no H I is detected in the observations at $r<4$ kpc. What H I is found in the well-known central hole has velocities which deviate strongly from our simple model (see Brinks, 1983). The regions outside 5 kpc in the model agree well with the observations both in velocity and in average intensity. The peak intensities on the observations occur at the crossings of main spiral arms with the major axis and, notably on the southern part of the major axis, are found at somewhat deviating velocities, typically differing from the model values by 10–30 $\mathrm{km\,s^{-1}}$, indicating streaming motions associated with these arms. Figure 4 also shows the model result for the cross-cut at 4.′8 W from the nucleus. Comparison with the observation at 4.′8 W shows reasonable agreement in velocity and in intensity of the disk in the outer parts. From about 0′ to 20′ N the H I shows three components, the warp and two disk structures. The splitting into two disk components occurs where the position-velocity map runs along the dust feature, labeled arm 3 by Baade. This feature, which is discussed by Bajaja and Shane (1982), lies at about 5 kpc from the centre.

Figure 6 shows by comparison with Fig. 5 which features in the position-velocity maps perpendicular to the major axis are due to the differentially rotating disk. All H I emission more than 18′ from the major axis is contributed by the warped layer. Inside 18′ the emission which is closest to the systemic velocity is from warped gas. The minor axis crosscut again shows the central hole in the H I and the presence of anomalous velocities. In fact, on the minor axis little H I is found at the expected systemic velocity (see Paper I) which means that the assumption of circular rotation is in some regards a poor simplification. The agreement, however, between the model and the observations for the main part of the disk, i.e. from about 4 to 16 kpc, is satisfactory. We use this model as the starting point for the more elaborate one which includes the warp.

4.3. Determination of the model parameters specifying the warp

In fixing the parameters specifying the warp we used the model by Henderson (1979) as a first approximation. In this model the warp is oriented such that the line of nodes of the warp is almost parallel to the major axis of M31. On the side of M31 near us, the north western side, the warp bends towards us and crosses the line-of-sight. The warp does not extend so far in that model as to cross the plane defined by the observer and the major axis (cf. Fig. 1). According to Henderson the warp starts at 16 kpc from the centre of M31 (in agreement with our value for R_d) and reaches a maximum height above the extended disk of 5.9 kpc. Qualitatively his model is able to explain the presence of two velocity structures in the spectra, one due to the disk and one due to the warp seen in projection onto the disk. A consequence of the Henderson model is that H I seen projected on the sky would only be found up to about 18 arcmin on each side of the minor axis. The new H I observations show, however, a diffuse H I envelope which extends to about 30 arcmin on both sides of this axis (see e.g. Fig. 9 in Paper I). This H I shares the same kinematics as the warped component seen projected closer to the nucleus (see e.g. Fig. 8 in Paper I) and evidently belongs to the same large-scale structure. This leads us to propose a flaring warp in which the scale height of the gas increases by a factor of about 10 in the outer parts with respect to the disk. Such a situation is similar to the one found in our Galaxy, where the H I scale height increases rapidly at large galactocentric radii (see e.g. Henderson, Jackson, and Kerr 1982; Kulkarni, Blitz, and Heiles 1982). Using a flaring warp and the modelling techniques we derive the following values for the parameters.

4.3.1. The extent, R_w, of the warp

The total extent of the M31 H I is about 30.5 kpc (Newton and Emerson 1977), so the warped part extends 14.5 kpc beyond the central disk.

4.3.2. The rotation curve, $V_c(r)$, at large radii

From studies of H I gas at large radii in other galaxies Sancisi (1983) found that at the onset of the warp the rotational velocities tend to decrease by about 5% to 20% and then again remain constant. Casertano (1983) and Bahcall (1983) showed that a decrease is expected for a galaxy with a truncated exponential disk as suggested by the photometry of van der Kruit and Searle (1981a,

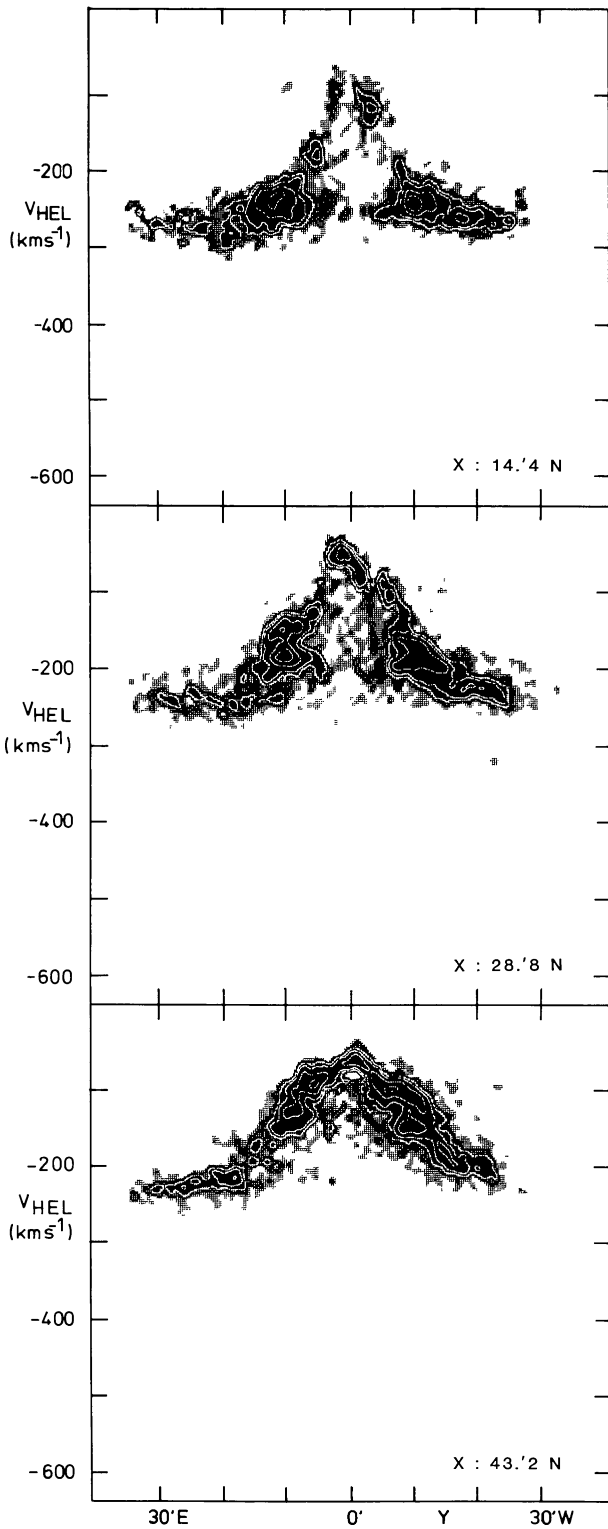

Fig. 5. Observed position-velocity maps made parallel to the minor axis of M31. (cf. Fig. 3)

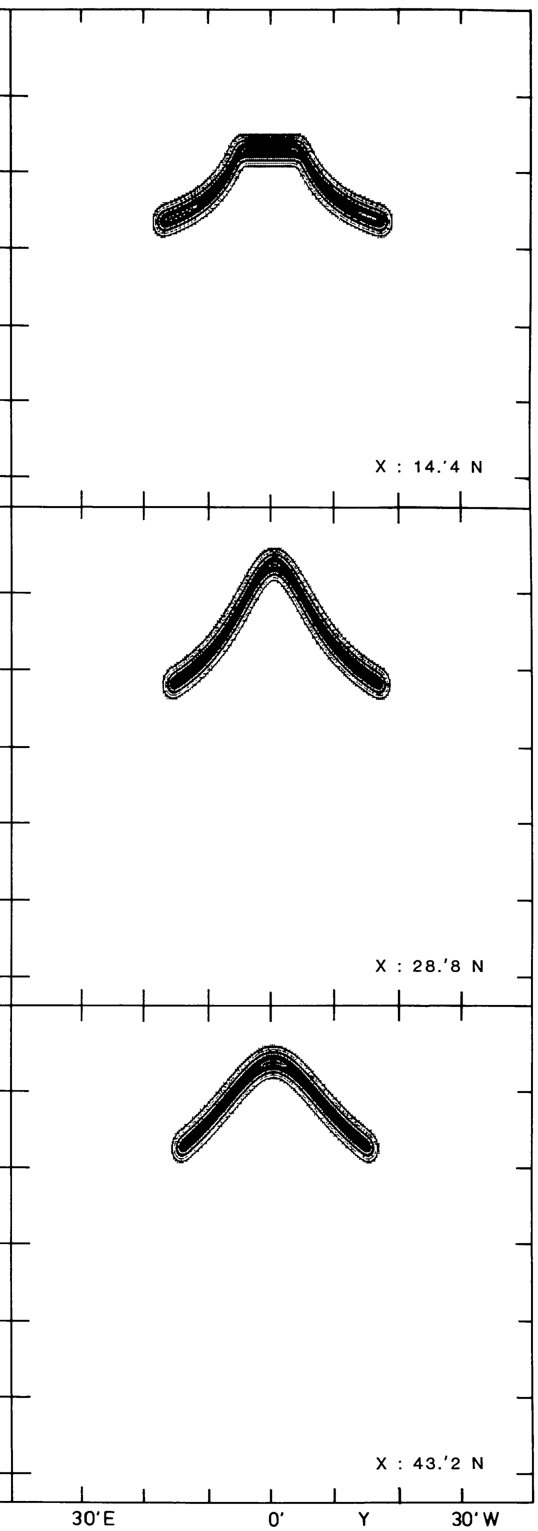

Fig. 6. Synthetic position-velocity maps produced from the initial flat-disk model described in the text and at the same locations as in Fig. 5. (cf. Fig. 3)

b) with the assumption of a constant M/L. The detailed shape of the rotation curve depends on the ratio of mass in the halo to that in the disk. A few runs were made with a model in which the rotational velocity was decreased at large R but the results proved to be only marginally affected by 10% changes in the velocity, mainly because the gas motions in the surveyed part of the warp are predominantly tangential to the lines-of-sight. We therefore decided to keep the rotation curve constant from 5.2 kpc out to the edge of the model. We realize that this flat rotation curve combined with our assumption of the rotation being parallel to the plane of the disk leads to a model in which the warp could plausibly lose its shape in about 10^9 yr due to differential precession. This is a problem which can best be addressed in dynamical studies of the maintainance of warps.

4.3.3. The maximum warp angle, ω_m

An estimate for the value of ω_m is obtained as follows. Little warped H I is seen projected onto the major axis. At larger Y H I is found out to about ± 30 arcmin. This means that the mean plane of the warp ends at a projected distance of about $Y = \pm 15$ arcmin. Additional modelling led to a value of $\omega_m = 15°$ with an estimated uncertainty of about 2°. This value for ω_m is smaller than the value of 25° deduced by Henderson. The maximum height of the mean layer above the extended disk is about 3.8 kpc, comparable to the value found in our Galaxy.

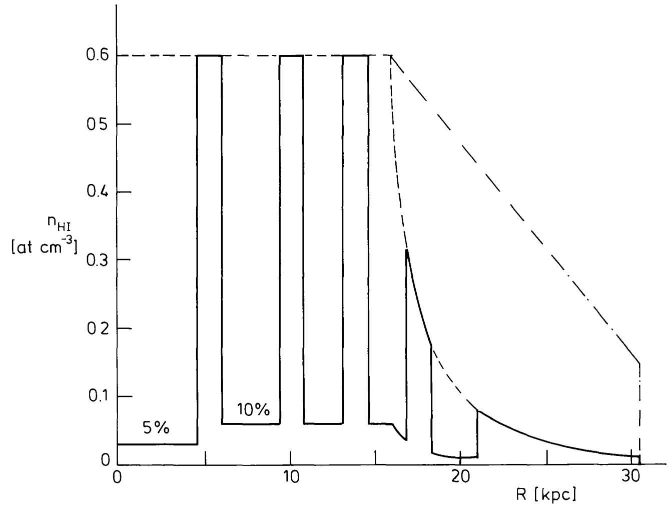

Fig. 7. The radial variation of the H I volume density at $z = 0$ as used in various models. The dot-dash line corresponds to the constant-scale-height warped case (see Fig. 8); the dashed line corresponds to the flaring warp case (see Figs. 10, 11, and 12). The full-drawn line corresponds to the case used to show the influence of high-contrast rings which are located approximately at the position of highest observed H I intensities (see Figs. 13 and 14)

4.3.4. The velocity dispersion and the gas temperature in the warp

Not much is known about the physical conditions of the gas in the parts of galaxies beyond the optical disks. Shostak and van der Kruit (1984) found the velocity dispersion in the inclined outer parts of NGC 628 to be constant at about 7–8 km s^{-1}. In our Galaxy Stark (1984) found a velocity dispersion of 8.2 ± 1 km s^{-1} for massive molecular clouds and 6.6 km s^{-1} for moderate mass clouds observed in the direction of the galactic anticentre. Crovisier (1978) found a value of 6.2 km s^{-1} for the dispersion of H I absorbing material in the solar neighbourhood. For the H I seen in emission the dispersion is somewhat less (Burton, 1976). In view of the large volume sampled by the telescope beam at the distance of M31, we felt that a value of $\sigma_g = 8$ km s^{-1} was reasonable. Lacking firm observational evidence to the contrary, we held σ_g constant. Similarly, we saw no reason not to hold the temperature constant at the value, $T_g = 125$ K, used in the disk.

4.3.5. The volume density, $n(r, z)$, of the warped H I layer

The surface density of H I drops at large radii. This is incorporated into the model by assuming that the surface density shows a linear decrease from the value it has in the disk to 25% of that value at the edge of the warp. Due to the increase of the scale height the volume density decreases much faster. Figure 7 shows volume density in the plane of the disk and the warp as a function of radius for a number of models.

4.3.6. The twist, γ_0, of the warp

Another parameter needed is the angle which the line of nodes of the warp makes with the line of nodes of the disk. The observations do not allow a determination of this angle as a function of distance in the warp. Observations of NGC 3718 and subsequent modelling by Schwarz (1984) show that in that system the line of nodes is straight, i.e. there apparently is no differerential precession. Numerical calculations by May and James (1984) of self-gravitating warps in disk galaxies also suggest that warps do not wind up in time. Based on these results we adopted in our model a constant twist, γ_0, independent of radius. We know from the model of Henderson (1979) and from the observations and model of Newton and Emerson (1977) that the warp of M31 is directed approximately into the direction of the line-of-sight, implying γ_0 is small. In our fitting, we made use of the integrated H I surface brightness maps published by Newton and Emerson in addition to the Paper I data. The Newton and Emerson data extend to larger radii measured along the major axis than the WSRT data. We also found that our position-velocity maps are not by themselves adequate to determine γ_0 because of the irregularities caused by arm segments which tend to be confused with asymmetries due to $\gamma_0 \neq 0°$. We therefore produced model maps of the integrated H I surface brightness and mean velocity field for the outer parts of M31 on the same scale as the maps published by Newton and Emerson. Model runs with $\gamma_0 = 0°$, $+10°$, $+20°$, and $+30°$ showed smaller changes as γ_0 changed. Comparison of the model runs with the observations led us to adopt a value of $\gamma_0 = +20° \pm 10°$ (estimated error). Model calculations with a twist of $-10°$, as proposed by Henderson, do not agree as well with the observations, predicting, among other characteristics, a warp which possesses a mild integral-sign shape opposite in sense to the one observed.

4.3.7. The scale height, $h(r)$, of the warped H I layer; introduction of a flaring warp

Our assumption of constant σ_g formally implies a gradual increase of the scale height (see van der Kruit, 1981). If at radii larger than the van der Kruit and Searle radius the density in the disk drops, we would expect a stronger increase of $h(r)$. An increase of the H I scale height was already inferred for the galaxy NGC 891 by Sancisi and Allen (1979). According to Sancisi (1983) the characteristics of the gas in spiral galaxies change around the edge of the old stellar disk and this is also where most of the observed warps begin. Kulkarni et al. (1982) derive for our Galaxy an almost linear increase in scale height outside the solar radius; the rms height

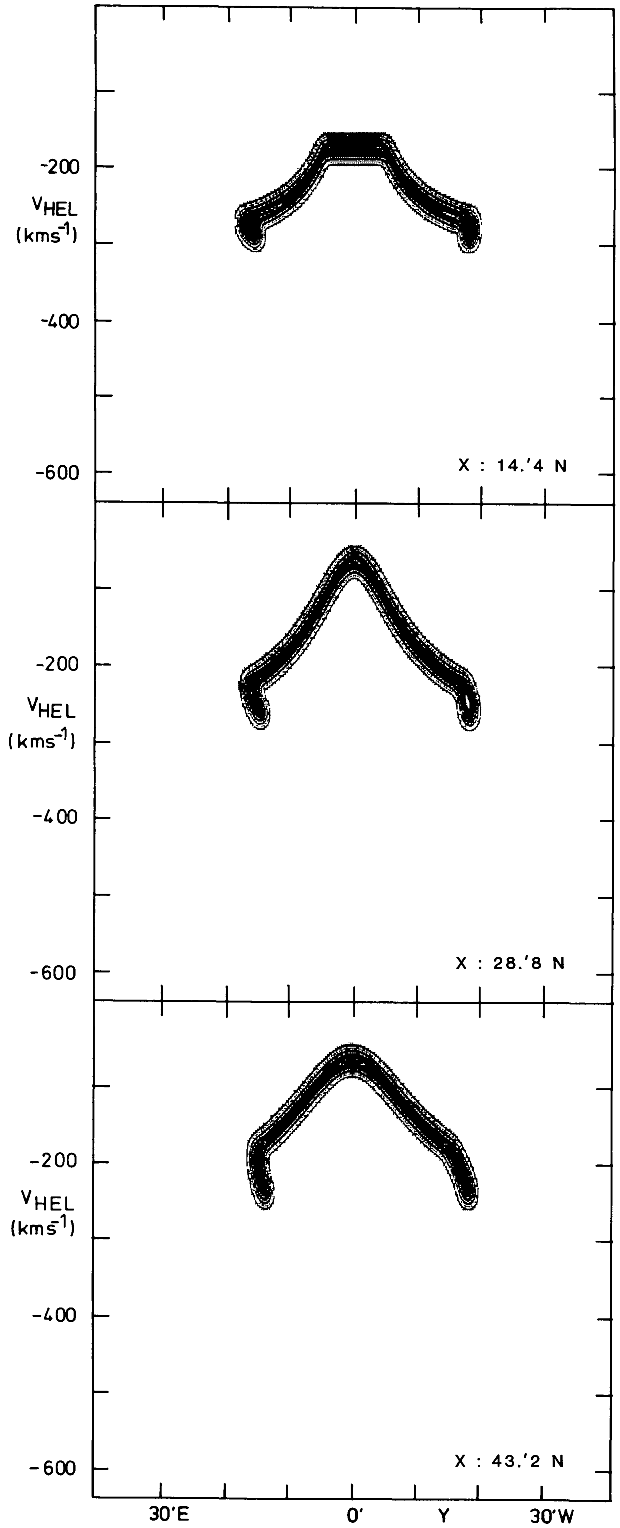

Fig. 8. Synthetic position-velocity maps parallel to the minor axis corresponding to the non-flaring warped gas layer case. (cf. Fig. 3)

above the mean plane of the warp increases from the local value to about 1.75 kpc. We initially held the scale height of the warped layer constant at the value of 120 pc found adequate in the disk. We subsequently found much improved fits if the thickness of the modelled warped layer increased linearly with radius. Figure 8 shows some model results for a disk plus warp for which the scale height of the gas is kept constant at a value of 120 pc. The double-peaked kinematic structure which is observed is hardly present in the modelled spectra, which show the double structure in a very limited region across the disk only. We first tried to improve the model by increasing the maximum warp angle, ω_m. By doing this our model became more similar to the tilted ring model of Henderson (1979). However, as long as the scale height of the warp was kept constant, we could not find values for the other parameters which led to adequate reproduction of the extent of the double-peaked structure and the visibility of the warp to 30′ on either side of the minor axis. This led us to introduce a flaring warp. We assumed that the scale height of the warped layer increased linearly with radius according to

$$h(r) = 120 + (r - 16.0) \times 108 \text{ pc} \qquad \text{for } r > 16.0 \text{ kpc}. \tag{13}$$

The flaring warp, and the maximum value of the scale height reached at the outer edge of the warped layer, about 1.7 kpc, recall the situation observed in our Galaxy.

5. Model of M31 based on a global flaring warp

Figure 9 shows in a face-on view the deviation of the midplane of the gas layer from the plane of the (extended) disk, $z_d = 0$. The deviation reaches a maximum value at the outer edge of the warp of 3.75 kpc. The relevant parameter values are summarized in Table 1.

Figure 10 shows the synthetic position-velocity major-axis cross-cut intended for comparison with the observations in Fig. 3. Evidently a small tip of the warp crosses the line-of-sight. At 4′.8 to the West of the minor axis we see that the model reproduces the

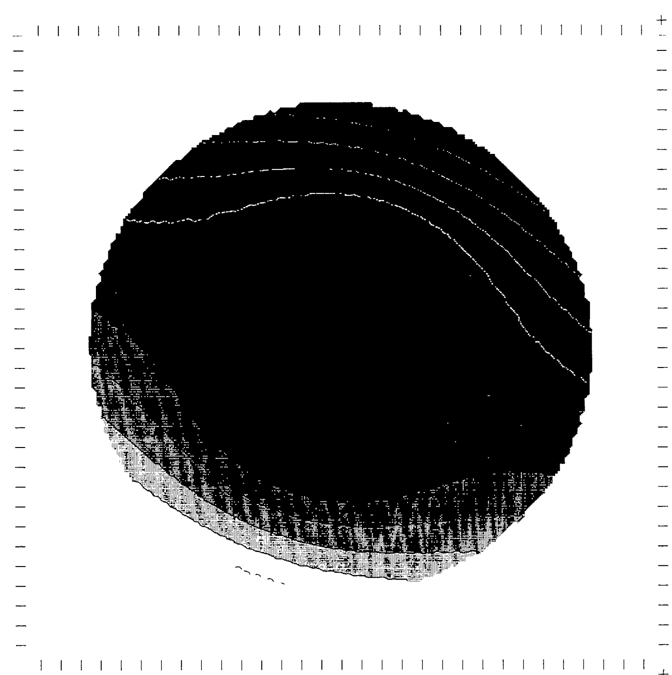

Fig. 9. Face-on view of the M31 model showing the deviation of the midplane of the warp from the midplane of the extended disk. The contour levels correspond to ±3, ±2.25, ±1.5, and ±0.75 kpc. The darker-grey shaded regions correspond to the part of the layer warped towards the direction of viewing, which is along the rotation axis from the south following side; from this direction the rotation is counter-clockwise

Table 1. Parameters of the flared warp model of the H I in M31

Distance to M31 (kpc)	$d=690$	
Radius of the disk (kpc)	$R_d=16.0$	
Extent of the warp (kpc)	$R_w=14.5$	
Inclination of the disk	$i=77°$	
Maximum warp angle	$\omega_m=15°$	
Twist angle of warp line of nodes	$\gamma_0=20°$	
Rotation curve (km s^{-1})	$V_c(r)=r\times 49.4$	$r<5.2$ kpc
	$V_c(r)=257$	$r\geqq 5.2$ kpc
Scale height of gas layer (pc)	$h(r)=120$	$r<R_d$
	$h(r)=120+(r-16)\times 108$	$r\geqq R_d$
H I volume density at $z=0$ pc (at cm^{-3})	$n(r,0)=0.6$	$r<R_d$
	see Fig. 7	$r>R_d$
Temperature of the gas (K)	$T_g=125$	
Velocity dispersion of the gas (km s^{-1})	$\sigma_g=8$	

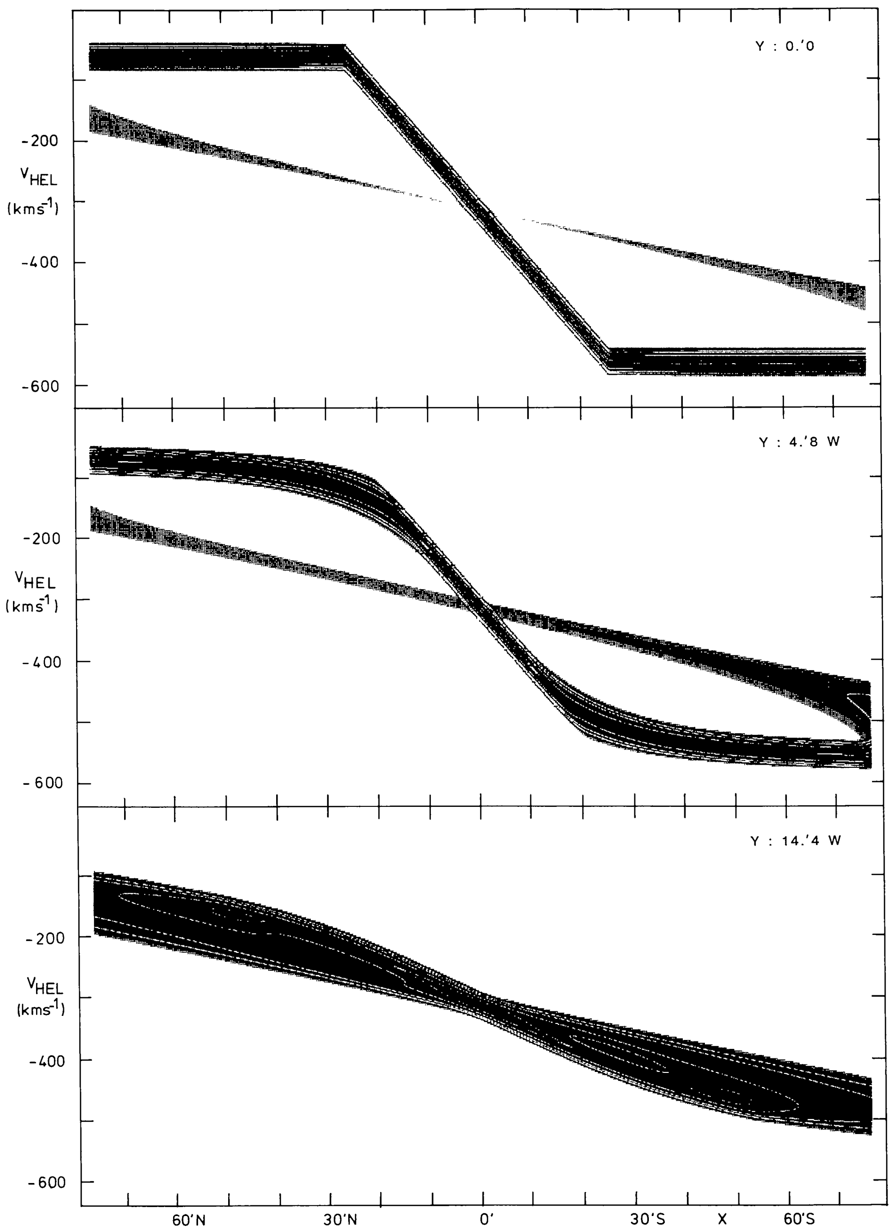

Fig. 10. Synthetic position-velocity maps parallel to the major axis corresponding to a smooth variation of H I density in the flared-warp case (cf. Fig. 3)

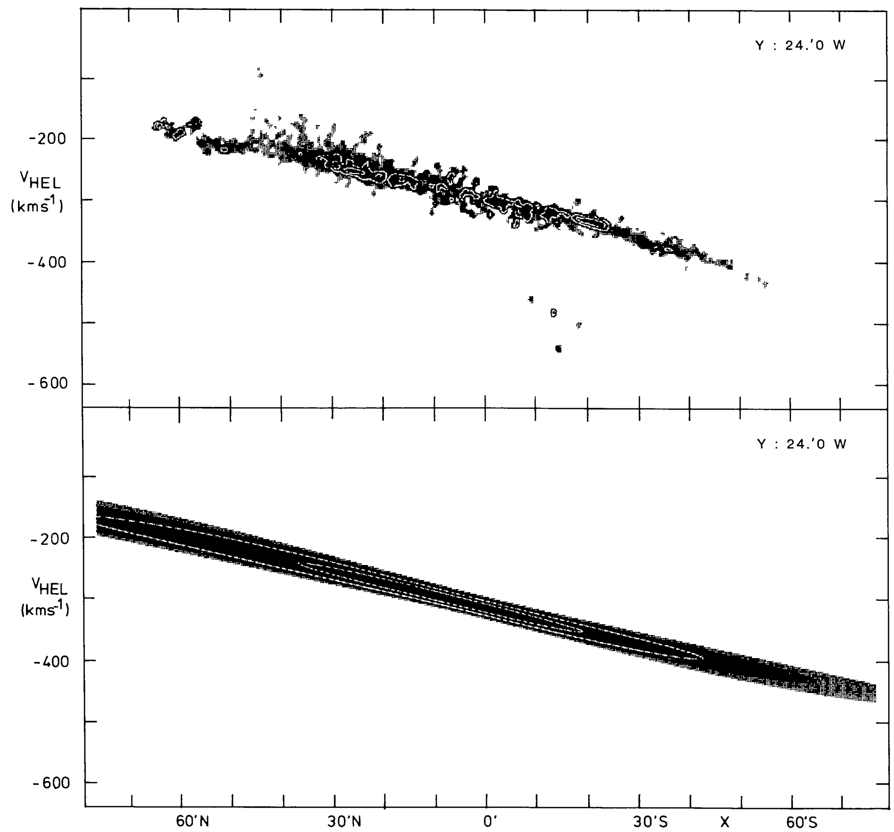

Fig. 11. Observed and synthetic position-velocity maps made along the line 24′ W of the major axis. The model profiles correspond to a smooth variation of H I density in the flared-warp case (cf. Fig. 3)

characteristic distorted figure-eight pattern of the observations. At 14.′4 W (Figs. 10 and 3, bottom panel) there is also reasonably good agreement of the model with the observations especially in the North. In the South the observations show a clear splitting where in the model the H I from the disk and the warp have blended in velocity to form one broad structure. At 24.′0 W of the major axis (Fig. 11) only one component is left in the model as well as in the observations. This component is contributed by gas at large distances from the nucleus and at $z_w \gtrsim 1.5$ kpc.

Figure 12 gives some example of position-velocity maps made perpendicular to the major axis. In these maps the pedestal features on either side of the major axis crossings are contributed by the gas in the warp. The broadening of the spectra as well as the faint tails in the position-velocity diagrams are well reproduced by the synthetic spectra. In Fig. 5, intended for comparison with Fig. 12, the lack of gas near the major-axis crossing for the cut made at 14.′4 N is due to the well-known central H I hole.

The models calculated above incorporated the simple variation of density with radius given by the dashed line in Fig. 7. We kept the density distribution simple in order to isolate the kinematic properties of the projected warped disk. With that done, we next introduced a more plausible density distribution. In what follows the H I volume density at $r < 4.8$ kpc was set at 5% of the maximum value at larger r. We introduced an additional variation of $n(r, 0)$ in order to investigate the possible influence of spiral arm segments on the appearance of the synthetic profiles. Questions concerning the number, location, and orientation of eventual arm segments in M 31 are generally unanswered, partly as a consequence of the unfavourable inclination of the system. Arms which have a small pitch-angle seem to form almost closed rings when seen under an angle of 77°. To imitate density variations due to spiral arms at least in a crude manner, we decided to treat the system as if it were build up out of rings. The arm to inter-arm contrast was set at 10 : 1. The location and width of the rings was read from the total surface brightness maps of Fig. 9 in Paper I, and, at large radii, from Unwin (1980b). The adopted run of $n(r, 0)$ is shown as a solid line in Fig. 7. In the following models no velocity perturbation was introduced which might be induced by these density variations; all other parameters were kept at the values listed in Table 1.

The consequences of introducing this density variation are evident in the synthetic maps shown in Fig. 13. Agreement with the observations is qualitatively good. The locations and relative intensities of the maxima and minima in the brightness temperatures in the synthetic position-velocity maps agree roughly with those in the observations. In Fig. 13 the splitting observed into two structures is also present in the model. In Fig. 14, representing the minor-axis cross-cut, the fit between model and observations has been improved by taking the central H I deficiency into account. Although the qualitative agreement of the flaring warp model with the observations is good, it is instructive to point out the areas in which the model might be improved. For example, the slope, in the position-velocity maps parallel to the major axis, of the warped gas seen projected close to the nucleus is slightly steeper in the observations than in the model (compare Figs. 3 and 13). Additional modelling showed that this slope is rather insensitive to changes in ω_m, because the warped H I is seen more or less edge-on. It similarly does not help to change the model such that the H I is forced to move in circular orbits which follow the warp instead of using the assumption of cylindrical rotation. Variation within the limits of plausible rotation velocities cannot reproduce the observed slope. For example, the drop in rotation velocities observed by Cram et al. (1980) and by Bajaja and Shane (1982) of about 30 km s^{-1} results in only minor changes. Large scale z-motions are not expected. Shostak and van der Kruit (1984) showed that in NGC 628 vertical motions are localized and generally less than a few km s^{-1}. Because of the orientation of the warp of M31, z-motions (if present) would only marginally influence the observations. A possible way to improve the model fit is to abandon circular orbits and allow the H I to move along elliptical streamlines. Because the warped H I on the minor axis is found at about the systemic velocity and because the slope in the position-velocity maps parallel to the major axis is steeper in the observations than in the model this would mean that the minor axis of the elliptical orbits would be roughly aligned with the line of nodes of the warp. Lacking both a firm observational foundation and a dynamical motivation for such elliptical orbits in M31, we did not abandon circular orbits.

A characteristic signature of the flared warp is found in the pedestals at low velocities in the position-velocity maps made perpendicular to the major axis. The pedestals displayed by the model (see Figs. 12 and 14) generally agree with those observed (see Fig. 5), but we found some regions where the warped H I pedestal observed differs significantly from the model. This suggests that the H I distribution in parts of the warp shows structure in the sense that either the local density is not constant or that projection effects lead to different column densities. We note that the North-East region contains the perturbed outer arm studied by Whitehurst et al. (1978) and by Sawa and Sofue (1982). It does not seem appropriate to complicate our global model to accomodate local perturbations. The global model has, however, given us sufficient confidence in the identification of the warped and unwarped regions of M31 that we have attempted to separate the contributions from them in the observations.

6. Separation of the H I emission from the warp and from the disk

6.1. Separation in the observations

The warp and the disk are evident as separate velocity systems over large portions of M31. The two systems share the same velocities near the minor axis. The modelling process has shown that, besides on the minor axis, the two systems also show the same radial velocities in the direction of the ring of maximum emission near 10 kpc. Except for these parts it is possible to see the warped H I separated from the normal disk H I. This allowed us to produce maps of the integrated surface brightness and the mean velocity separately for the two components.

To separate the components the position-velocity maps which were made parallel to the major axis were displayed on the Leiden image processing system. They were inspected in rapid sequence, in order to recognize the spatial continuity between features in consecutive maps. Masks were produced for sets of about ten to twenty consecutive cross-cuts. One mask was chosen to select emission contributed by the warp and a second mask to select emission contributed by the disk. Around the minor axis and in some areas at about 10 kpc from the centre the two masks overlapped. Corrections for the inclusion of emission which is present in both masks are applied later. The masks were applied to all cross-cuts available from the Paper I data. Each set of position-velocity maps was thus divided into a set of warp cross-cuts and a set of disk cross-cuts. Each set of cross-cuts was then transformed back to channel-map form. These channel maps were then used to produce integrated surface brightness maps and

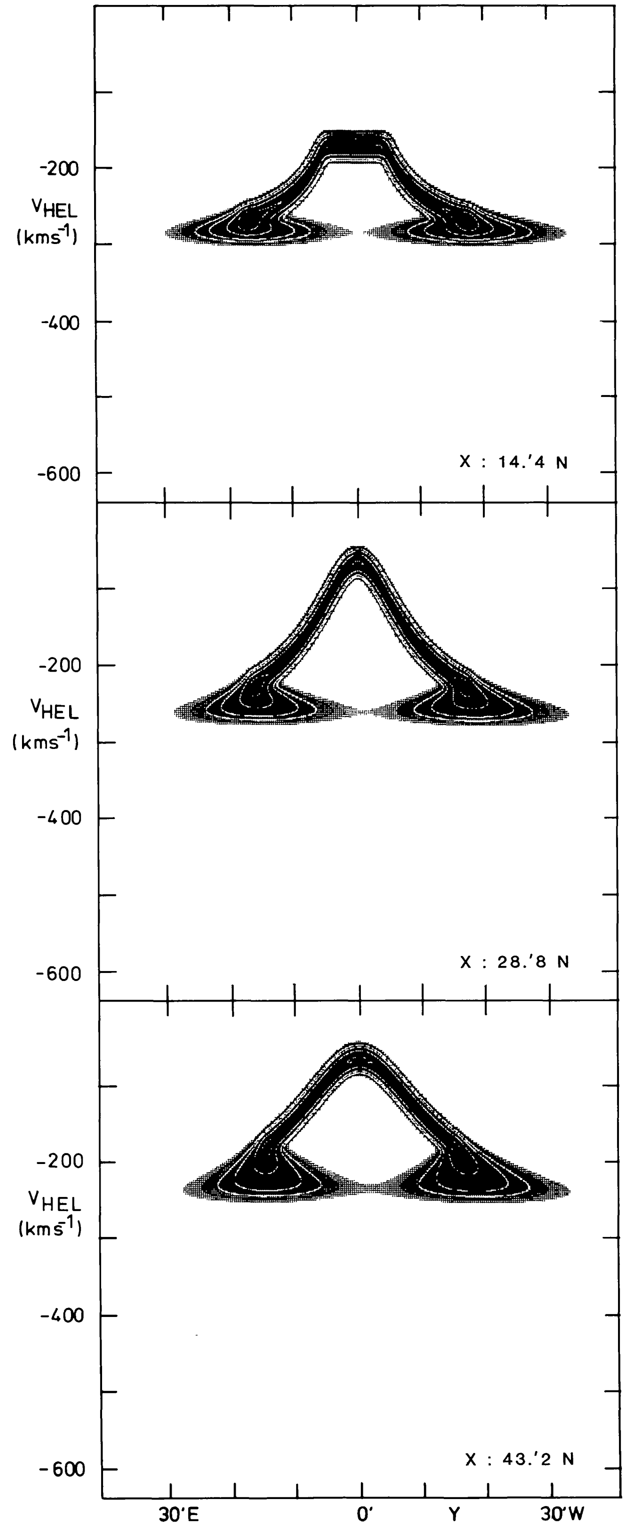

Fig. 12. Synthetic position-velocity maps parallel to the minor axis corresponding to a smooth variation of H I density in the flared-warp case (cf. Fig. 5), and showing the pedestal signature characteristic of the flaring and required by the observations. (cf. Fig. 3 for the contour and grey-scale levels)

a mean velocity field for each component. Figure 15 shows the integrated H I map and the velocity field of the unseparated observations. The contour delineates the area in which H I from the warp and the disk cannot be separated. Figures 16 and 17 show

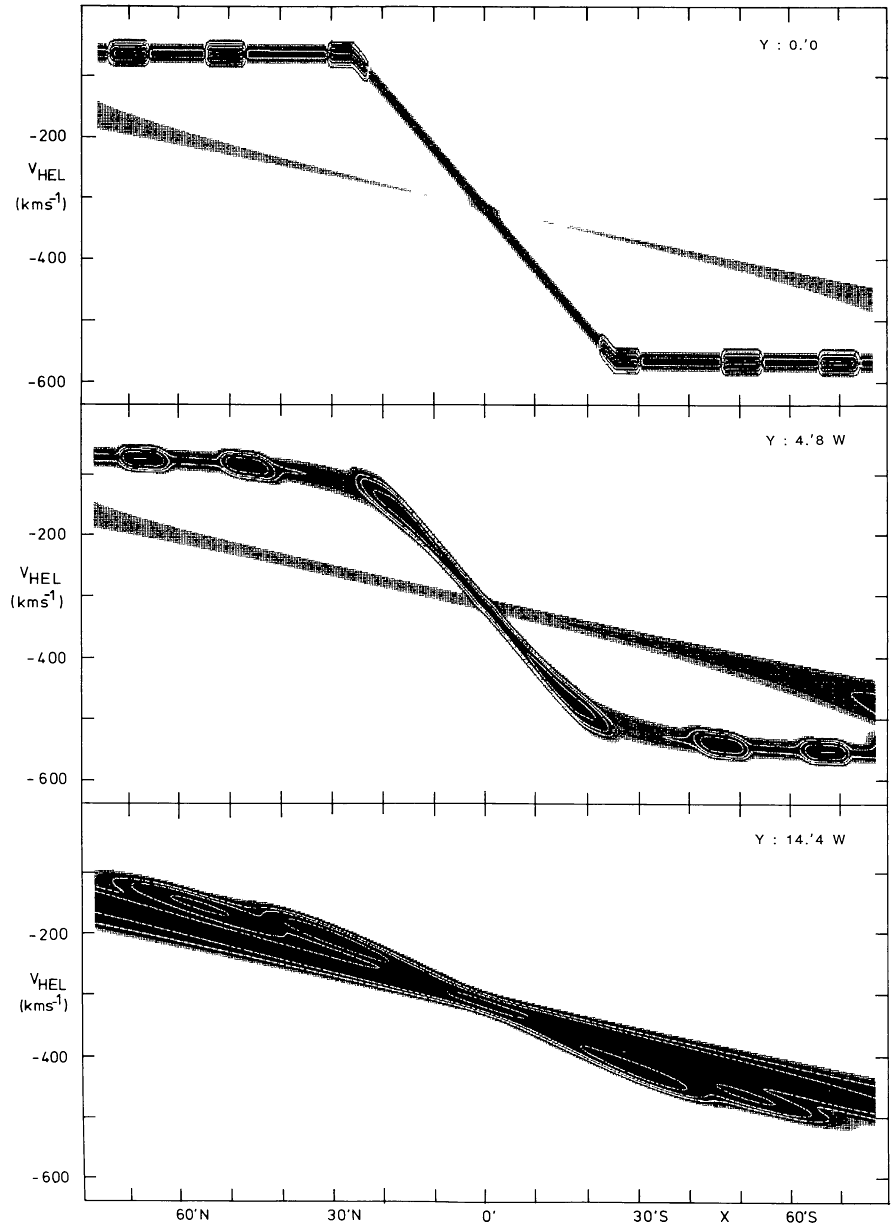

Fig. 13. Synthetic position-velocity maps parallel to the major axis using the high-contrast H I density shown in Fig. 7 and a flaring warp. (cf. Fig. 3)

the integrated surface brightness map and the velocity field for the disk and warp components separately.

It is natural to ask which fraction of the total H I mass resides in the warp and which in the disk. Assuming optical thinness and converting the total integrated intensities into H I column densities yields an H I mass $M_{H_I}(\mathrm{WSRT})=2.74\ 10^9\,M_\odot$ for the observed WSRT area. This value corresponds to the emission shown in Fig. 15. It can be compared with the value of $M_{\mathrm{H_I}}(\mathrm{Bonn})=3.86\ 10^9\,M_\odot$ derived by Cram et al. (1980) from their survey, which has greater sensitivity at large radii along the major axis. The WSRT survey covered about 25% of the total area outlined by the lowest contour of the integrated H I map given by Cram et al. About 71% of the total H I is contained within the WSRT survey area. Our modelling produced a ratio in rough agreement with this. Integrating the model over the area covered by the WSRT survey gives about 65% of the total H I. The warped component has an H I mass of $M_{\mathrm{H_I}}(\mathrm{WARP})=1.68\ 10^9\,M_\odot$, uncorrected for the H I in the region of overlap with the disk component. The disk component has a mass of $M_{\mathrm{H_I}}(\mathrm{DISK})=2.16\ 10^9\,M_\odot$. Comparison with the total mass observed with the WSRT shows that the overlap regions contain about 1.10 $10^9\,M_\odot$ of H I.

We can use the modelling results also to estimate the ratio of H I mass in the warp to that in the disk after correction for the H I in the overlap regions. This procedure, which is possible because the modelled and observed intensities agree quite well went as follows. The modelling resulted in maps (Figs. 18a and 19a) of the total surface brightness of the disk and the warp. The H I masses for the warp and the disk derived from these maps are W^T and D^T. From these maps we selected the area which had been observed with the WSRT and determined the mass of the H I in the warp and the disk in that area, W^A and D^A. Finally the overlap area which resulted from the separation of the components was excluded from the model, giving W^0 and D^0. The mass ratios derived in this way are $W^0:W^A:W^T=17:30:53$ and $D^0:D^A:D^T=16:42:42$. The

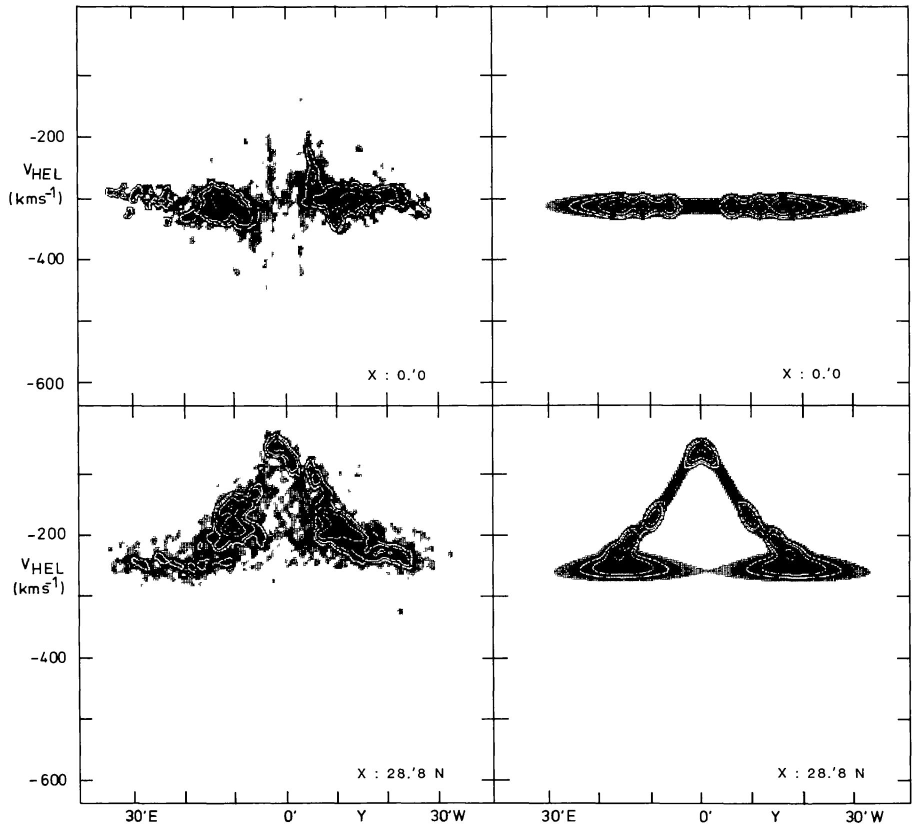

Fig. 14. Observed and synthetic position-velocity maps made parallel to the minor axis. The model has the high-contrast H I density shown in Fig. 7 and a flaring warp

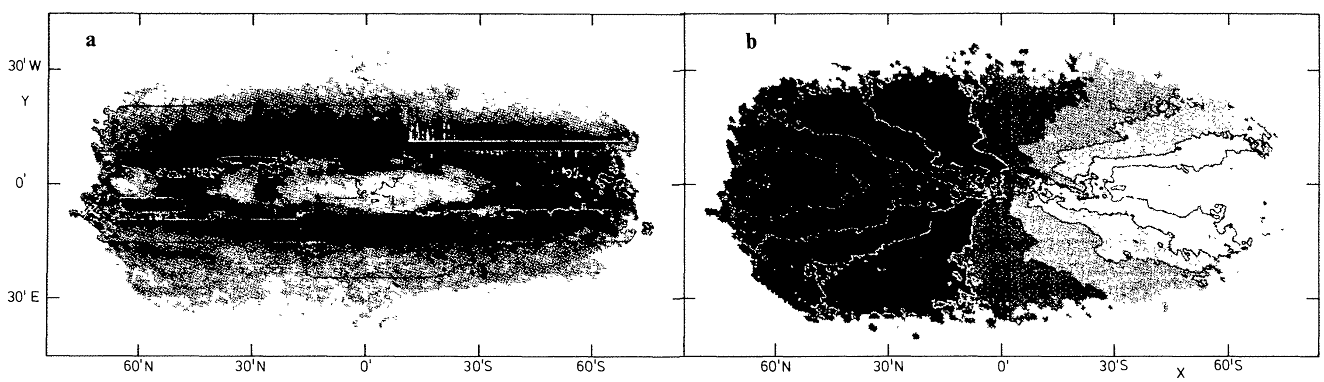

Fig. 15. a Surface density of the total H I, including both the disk and warped components of M31. The contour delineates the regions of overlap where it is difficult to separate the disk emission from the warp emission. The resolution of the data is $\Delta\alpha \times \Delta\delta = 48'' \times 72''$. **b** Velocity field of the total H I distribution, showing the intensity weighted mean velocity. The contour levels are -100, $-160, \ldots, -580$ km s^{-1}. The same contour and grey-scale levels are used for Figs. 15 to 19

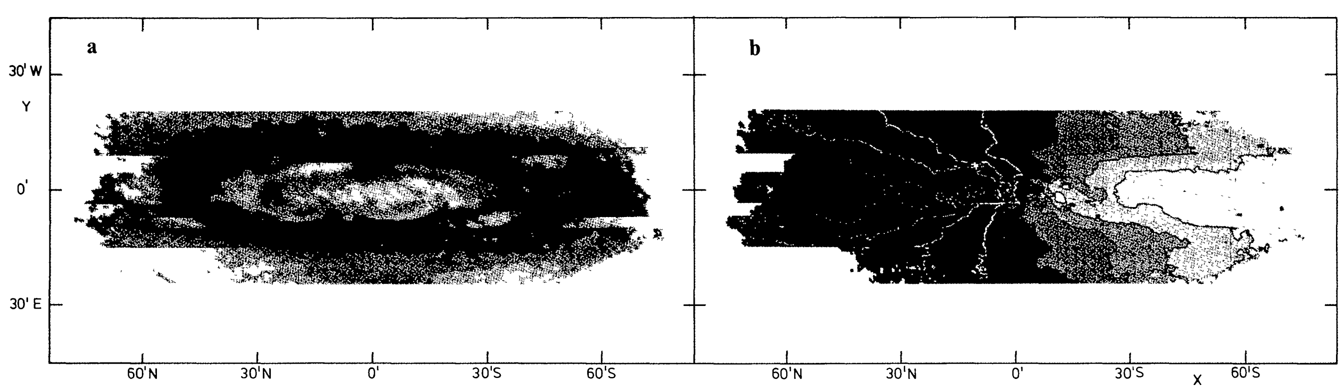

Fig. 16. a Surface density of the disk H I, derived after separation of the warped and disk components. **b** Corresponding velocity field of the disk H I (cf. Fig. 15)

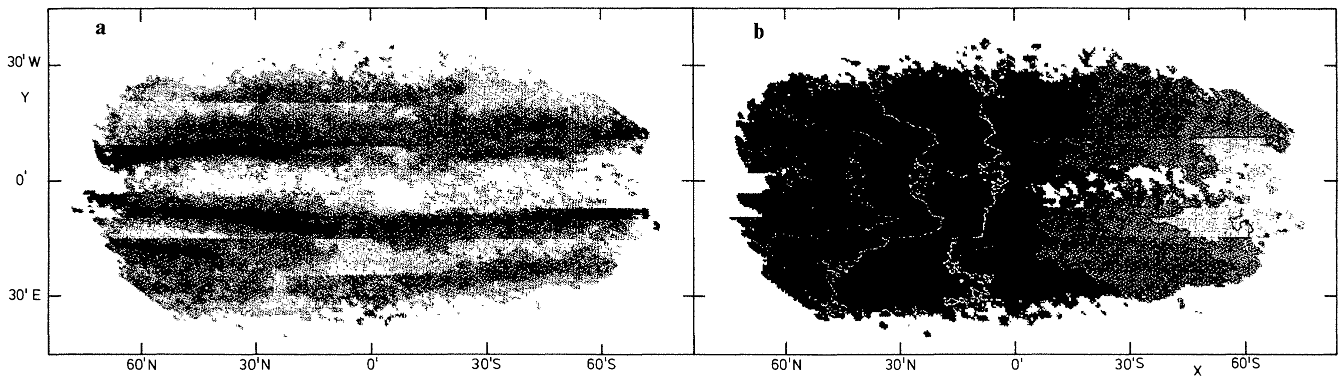

Fig. 17. a Surface density of the warped H I derived after separation of the warped and disk components in the manner discussed in the text. **b** Velocity field of the warped H I, derived after separation of the warped and disk components (cf. Fig. 15)

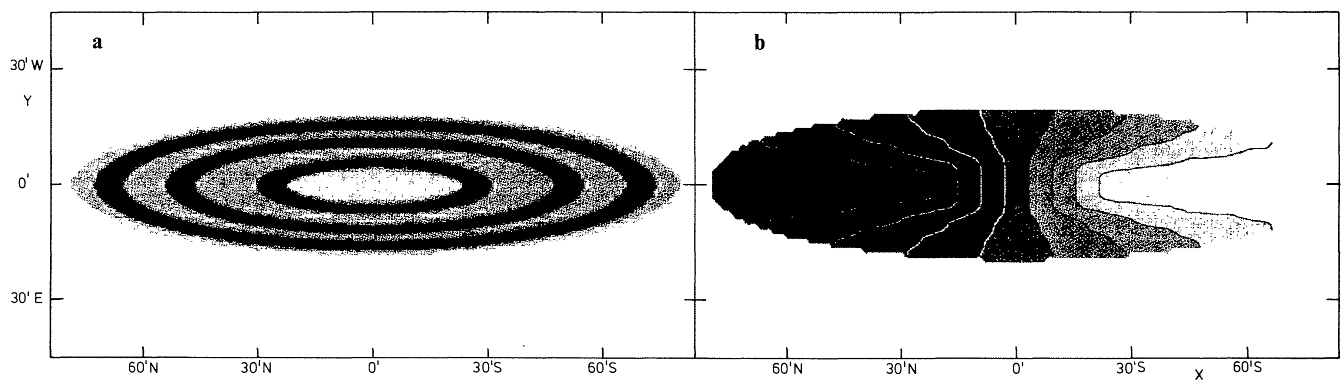

Fig. 18. a Surface density map of the disk part of the model, i.e. at $r \leq 16$ kpc, made using the high-contrast density distribution given by the full drawn line in Fig. 7. **b** Velocity field of the disk part of the same model. The contour and grey-scale levels are similar to those used for the observations (cf. Fig. 15)

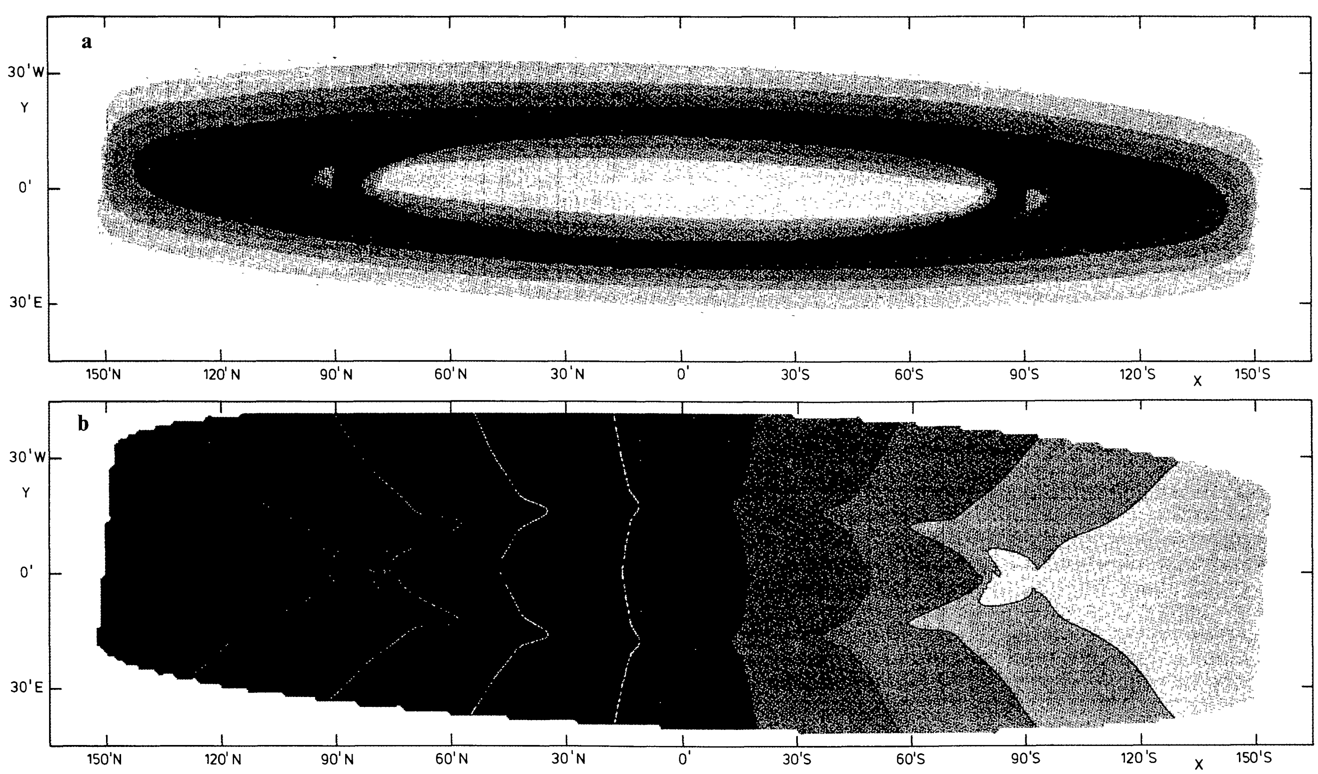

Fig. 19. a Surface density map of the warped part of the model, i.e. at $r \geq 16$ kpc, made using the high-contrast gas density distribution of Fig. 7. **b** Velocity field of the warped part of the same model (cf. Fig. 15)

observed amount of H I, excluding the overlap areas, is 0.58 $10^9 M_\odot$ for the warp and 1.05 $10^9 M_\odot$ for the disk, so that the observed $W^0:D^0$ ratio is 35 : 65. Assuming that the above ratios, derived from the model, apply to the observations, we can use them to calculate $W^A:D^A=27:73$ and $W^T:D^T=39:61$. The integrated H I maps shown in Figs. 16 and 17 have been corrected for the excess H I in the overlap region by reducing the surface brightness in the overlap areas of the raw warp and disk maps to 27% and 73% respectively of their original values. By doing this the total amount of H I in the disk and warp is brought into accord with the total mass derived above for the WSRT survey. The detailed structure of the H I in the overlap areas can not, however, be separated into contributions by the warp and the disk, and any interpretation of the H I distribution within the overlap regions should be made with caution. Because the velocity fields of the warp and disk in the region of overlap are similar, no correction is needed.

6.2. Kinematic and structural properties of the warp and the disk

Figure 15b shows the mean velocity field which follows from a straightforward determination of the intensity-weighted mean velocity of each observed H I profile. The separated velocity fields are remarkably different from this mean velocity map and from each other. The observed disk velocity field, Fig. 16b, shows the familiar signature of differential rotation. In the inner parts, at $r<5$ kpc, we see the contribution of the anomalous-velocity H I. Associated with the main arms are small-scale kinematic irregularities, such as the wiggles on the north-western side which correlate with the dust arm (arm 3). At larger galactocentric distances the disk velocity field becomes quite regular. The observed field of the warp, Fig. 17b, differs strongly from that of the disk. The velocity gradient in the inner part of the warp is less steep than in the disk; the overall impression is of a velocity field with the signature of a ring in circular rotation. It seems clear that without knowing the relative importance of the warp and disk components it would not be possible to make proper use of the mean velocity field map in Fig. 15b. Many details, in particular of the disk in the inner 5 kpc of M 31, are lost or contaminated by the presence of the two systems.

The model velocity fields and integrated surface brightness maps which were derived are given by Figs. 18 and 19 which show the results separately for the disk and for the warp. We include in the maps for the warp emission from all of M 31, even from that outer portion which is absent from the WSRT data. The model velocity field for the disk agrees reasonably with the one observed, except for the anomalous features near the centre. The model field for the warp accounts for the global properties of the observed map. The wiggles in the model velocity field of the warp in Fig. 19b are not due to streaming motions but are a consequence of the geometry of the model and the rather complicated projections involved. Because so many aspects of the observations seem to require a geometry of this sort, we find it plausible to interpret in the same way the wiggles observed in the warp and evident in Fig. 17b.

The integrated surface brightness maps of the disk and of the warp, Figs. 16a and 17a show that the H I distribution in M 31 is not symmetric. On the southern major axis there is a lack of H I relative to the northern part. The data show that, for the area covered by the WSRT survey, 62% of the H I mass is found in the northern half and 38% in the southern half of M 31, in agreement with the earlier observations of Davies and Gottesman (1970). Because the asymmetry is North-South it can not be attributed to a twist of the line of nodes of a sinusoidally-varying warp. This mildly lopsided distribution of H I is of the same sort but less pronounced as those reported by Baldwin et al. (1980) for a number of other nearby galaxies.

As is the case with the velocity-field map of the disk, most clarity is gained in the integrated surface brightness map (Fig. 16a) in the inner 5 kpc. Here the extended structures stand out more clearly after substraction of the warped gas. Especially the dust arm is more pronounced. A more detailed discussion of the anomalous H I velocity and the H I distribution in the inner 5 kpc is in preparation (Brinks, in preparation). Comparing Figs. 16a and 18a shows that the density structure of M 31 incorporated in our model is only a crude approximation to reality. But we do not see how a great number of additional structural parameters would increase our understanding of the gas-layer morphology.

The H I distribution in the warp shows some small scale structure. The most prominent feature is the arm segment in the North-East referrred to by Whitehurst et al. (1978) and by Sawa and Sofue (1982) as the perturbed outer arm. As we have already seen in the discussion of the position-velocity maps, this arm follows the velocities expected for the warped H I. The arm-interarm intensity contrast is about 4 : 1. At the position of this arm segment Pellet et al. (1978) found no H II regions. There are some indications that there are other arm segments and extended structures in the warp, but the interpretation is severely hampered by the unfavourable inclination of M 31 and by the almost completely edge-on presentation of the flaring warp. It is at least clear that the H I gas in the warp is not featureless, a point which is strngthened by the observations of Shostak and van der Kruit (1984) of the face-on galaxy NGC 628, which show spiral structure out to the edge of the observed field, deep into the warped parts.

7. Comparison with other galaxies and with models

7.1. Comparison of the M 31 warp with that of our Galaxy

The morphology of the gas layer in M 31 has roughly the same form as that determined for our Galaxy. The gas distribution in the outer Milky Way has most recently been studied by Henderson et al. (1982) and by Kulkarni et al. (1982). For our purposes, the principal difference between these two studies lies in the rotation curve adopted. Henderson et al. considered the rotation speed constant, at the solar value, outside the solar circle; Kulkarni et al. followed indications from studies of CO velocities and H II region distances and allowed the rotation speed to rise before becoming constant at $R=19$ kpc with a linear velocity of 285 km s^{-1}. The linear dimensions which we compare with M 31 are taken from Kulkarni et al. The outer perimeters of both galaxies then occur at about 30 kpc, but the onset of the warp in our Galaxy occurs at a smaller radius than in M 31. In our Galaxy, the maximum deviation above and below the galactic equator is reached at a galactocentric longitude of about 85° and 265° respectively; approximately in the directions of the galactic centre and anticentre the deviations from $b=0°$ are minimal. The regular variations throughout the warps and the 2π-symmetries suggest that they are globally induced phenomena.

The warps in both M 31 and in our Galaxy show approximately equal amplitudes. The maximum-warp-angle parameter, ω_m, is a measure of this amplitude which is independent of the adopted distance scale. From Fig. 2 of Henderson et al. we find that the midplane of the gas layer rises at an angle of about 14°. Our model of M 31 adopted $\omega_m=15°$. The warps in both M 31 and in our Galaxy flare. Figure 6 of Kulkarni et al. shows that the observations in our Galaxy require a scale height increasing linearly to a maximum value of about 1.7 kpc at $R \sim 30$ kpc. Our model of M 31 led to a similar value. Because the midplane volume density used in the model is similar to that found for our Galaxy, the comparable scale heights imply that the mass surface density of H I in the outer parts of the two galaxies falls off with R in approximately the same way. The arguments used by Kulkarni et al. apply also to M 31: the linearly increasing scale height implies that the large mass required by the flat rotation curve can not reside in a thin disk.

Comparison with the situation in our Galaxy leads us to comment briefly on the gas parameters of temperature, density, and velocity dispersion. The values which we gave to these parameters (125 K, 0.6 cm^{-3}, 8 $\mathrm{km\,s}^{-1}$) are similar to the ones which have proven adequate for coarse, one-component structural and kinematic descriptions of the basic H I layer in our Galaxy. We know that the interstellar medium contains a wide range of temperatures and densities. Information on the details of the physical state of the gas has been derived mostly from studies of the solar neighbourhood or from H I absorption studies which sample a very small volume. Few H I features at distances corresponding to galactic scales can be studied individually; as a group they are organized in a coherent layer whose scale height, gross optical depth properties, and kinematics can be studied. The rather ubiquitous distribution of H I and the large volumes intercepted by the telescope beam results in the accumulation of emission and absorption characteristics of probably unrelated material at overlapping velocities in single profiles. But it remains the case that a one-component model is able to mimic the global H I properties in M 31 as well as in our Galaxy. This could serve to constrain models of the interstellar medium, in particular regarding the frequency and size of very cold, opaque clouds and the frequency and size of hot and diffuse, or empty regions. Very little such work has been done.

7.2. Comparison of the M 31 warp with that of other nearby galaxies

The third large spiral in the Local Group is M 33. The integrated H I surface brightness map of this galaxy shows a rather vague integral-sign shape (see Wright et al., 1972). Sandage and Humphreys (1980; cf. Bosma, 1983) found that the faint outer optical structure could be rectified to a more regular pattern if account were taken of a warp of the outer regions. The most comprehensive work on demonstrating a warp in M 33 is that of Rogstad et al. (1976). They noticed that the H I spectra typically show a more complicated form than one would expect of a single traverse of the line-of-sight through a simple gas layer. They showed that an extra component would be introduced into the H I spectra by a model of tilted thin rings in which the outer rings of M 33 are viewed progressively more edge-on, until they cross the lines-of-sight through the inner parts. Their model of M 33 is thus quite similar to the later ones of M 31. That the rings are thin does, however, require a very severe warping of the plane. A milder degree of warping would be required by a model in which the scale height of the H I layer is allowed to increase at large radii as it does in M 31 and the Galaxy. A detailed WSRT H I survey of M 33 has recently been completed and is currently being reduced by E.R. Deul in Leiden, and will be subject to synthetic-profile modelling.

The general characteristics of the M 31 warp are similar to those of the warps found in a number of nearby galaxies reviewed by Sancisi (1983). The shared characteristics include (i) the location of the onset of the warp close to the optical boundary (in M 31 the Holmberg radius is 19.8 kpc); (ii) the tendency for the rotational velocity to drop slightly at the onset of the warp; (iii) the strong increase with radius within the warp of the gas layer scale height, and (iv) the decrease with radius of the density. Regarding the density profile we note that for a situation like that in M 31 the averaged H I surface density will not yield a correct radial distribution of density (cf. Unwin, 1980a, b; Sofue and Kato, 1981) unless explicit account is taken of the viewing geometry. The modelling shows that the shoulder in the total surface density distribution at radii 12–15 kpc and the abrupt drop at larger radii are due to projections of the warped layer onto the disk.

Because the warps are observed to flare in the two best-studied cases, it is natural to ask if flaring is not a general property of global warps. It is important to test this suspicion in other cases because of the implications to the total mass distribution and consequently to the dynamics in warped galaxies. The appearance of global warps in the three large spirals in the Local Group and in several nearby spirals suggests that warps are a common characteristic of spiral galaxies. The additional material which is most important for an accurate determination of the frequency of occurrence of warps is detailed spectral line maps. The kinematic information is important because, in general, the integrated surface brightness of a galaxy with a global warp will not show a well-defined integral-sign signature. (This conclusion holds even for more or less edge-on galaxies). For example, the model warp for M 31 shown in Fig. 19 does not show such a signature. The evidence for a global warp in M 31 comes almost entirely from the two-component structure of the spectra. Presumably detailed kinematic information will reveal evidence for warps in other galaxies which are on the basis of total surface brightness contours not now recognized as warp. An example of another system in which a warp is inferred on the basis of the kinematic information is the galaxy NGC 3718 (Schwarz, 1984).

7.3. Possible influence by the companion galaxy M 32

No consensus has yet been reached regarding the cause and maintenance of galactic warps. Observationally based investigations such as this one can provide some useful phenomenological constraints on dynamical models. The frequency of occurrence of global warps indicates that such warps are common. The discovery of very isolated warped galaxies, such as NGC 5301 (Krumm and Shane, 1982; Huchtmeier and Richter, 1984) and others discussed by Sancisi (1983) indicates that such warps are not the consequence of interactions with neighbouring galaxies.

Whether the distortions of the M 31 ga layer could be locally induced by tidal interaction with the small elliptical companion M 32 has been considered in a series of papers by Byrd (1976, 1977, 1978). Byrd modelled the interaction in such a way that multiple-peaked H I spectra would result as well as structured distortions in the gas layer. Comparison of the figures given by Byrd (1977) with the observed situation is instructive. Although Byrd's model is able to generate a two-component velocity field which is in reasonable agreement with the data in a region South of the nucleus, the perturbations are confined to a much smaller region in the model than in the observations. The gas sheet ejected from M 31 by the passage of M 32 is present only in the range $50'\mathrm{N} < X < 50'\mathrm{S}$, whereas the observations show double-peaked profiles over essentially the entire galaxy. Because only a limited portion of the M 31 disk is distorted in Byrd's simulation, the predicted effects differ much more dramatically on opposite sides of the axes in contrast to the substantial symmetry observed. The amount of H I in the non-disk component is some $10^9 M_\odot$; although the interaction model can be modified by adjusting the unknown distance between M31 and its companion, this seems like a large mass to result from a tidal forcing (cf. Hunter and Toomre, 1969). In general the model also poorly represents the velocity field of the non-disk component, which is observed to be extremely regular. The 2π-symmetry and general regularity of the warp in M31 argue against it being a consequence of interaction with M32.

8. Conclusion

The following conclusions result either from our modelling of the Brinks and Shane (1984) WSRT H I observations of M31 or depend on a wide range of earlier work by others but to which the modelling gives additional support.

1. The large-scale H I distribution and kinematics in M31 can be modelled by the global, flaring warped gas distribution described by the parameters in Table 1.
2. The scale height of the warped part of M31 increases approximately linearly with radius. The pedestals in position-velocity maps parallel to the minor axis indicate this flare (Figs. 12 and 14). The maximum deviation of the warp from the plane of the (extended) disk is about 3.8 kpc. The maximum scale height of the gas at the outer edge of the warp is about 1.7 kpc.
3. The flaring gas layer and flat rotation curve characterizing the outer regions of M31 require that the mass there resides in a halo.
4. Separate identification of the velocities contributed by the flat disk and by the flaring warp allows determination of the velocity fields and H I mass distributions for these components (Figs. 16 and 17). The total amount of H I mass in the disk is about $2.4\ 10^9 M_\odot$; the H I mass in the warp is about $1.5\ 10^9 M_\odot$.
5. The parameters specifying the global, flaring warp in M31 are similar to those specifying the warp in our Galaxy.
6. The same gas temperature, density, and velocity dispersion parameters which are useful for coarse descriptions of the H I in our Galaxy may be used in M31.
7. A well-defined integral-sign signature in the outer integrated intensity contours is not generally expected for a global warp of the sort seen in M31 or in our Galaxy. The kinematic behaviour revealed by detailed H I surveys will probably prove the most useful tool for studying global warps.
8. The 2π-symmetry and general regularity of the warp in M31 argue against it being a consequence of interaction with the small elliptical companion M32.
9. The frequency with which warps occur suggests that they are common; their regularity and occurrence in isolated galaxies suggest that they are not the consequence of interaction with nearby galaxies.

Acknowledgements. We are grateful to Drs. A. Bosma, E. Deul, T. de Zeeuw, and especially C. Norman and W. Shane for useful discussions and for their comments on an earlier version of this manuscript. Mrs. H. Versteege-Hensel assisted at various stages of the project. The photographs were prepared by Mr. W. Brokaar and the drawings by Mr. J. Ober.

The WSRT is operated by the Netherlands Foundation for Radio Astronomy (SRZM). E.B. was supported by the Netherlands Foundation for Astronomical Research (ASTRON). Both foundations are supported financially by the Netherlands Organization for the Advancement of Pure Research (ZWO).

References

Arp, H.: 1964, *Astrophys. J.* **139**, 1045
Baade, W.: 1963, Evolution of Stars and Galaxies, ed. C. Payne-Gaposchkin, Harvard U.P., Cambridge
Baade, W., Arp, H.: 1964, *Astrophys. J.* **139**, 1027
Bahcall, J.N.: 1983, *Astrophys. J.* **267**, 52
Bajaja, E., Shane, W.W.: 1982, *Astron. Astrophys. Suppl.* **49**, 745
Baldwin, J.E., Lynden-Bell, D., Sancisi, R.: 1980, *Monthly Notices Roy. Astron. Soc.* **193**, 313
Bosma, A.: 1981a, *Astron. J.* **86**, 1791
Bosma, A.: 1981b, *Astron. J.* **86**, 1825
Bosma, A.: 1983, in *Internal Kinematics and Dynamics of Galaxies*, IAU *Symp.* No. 100, ed. E. Athanassoula, Reidel, Dordrecht, p. 11
Brinks, E.: 1983, in *Internal Kinematics and Dynamics of Galaxies*, IAU *Symp.* No. 100, ed. E. Athanassoula, Reidel, Dordrecht, p. 27
Brinks, E., Shane, W.W.: 1984, *Astron. Astrophys. Suppl.* **55**, 179
Brouw, W.N.: 1975, in *Methods in Computational Physics* **14**, 131, eds. B. Alder, S. Fernbach, and M. Rotenberg, Academic Press, New York
Burke, B.F.: 1957, *Astron. J.* **62**, 90
Burton, W.B.: 1971, *Astron. Astrophys.* **10**, 76
Burton, W.B.: 1976, *Ann. Rev. Astron. Astrophys.* **14**, 275
Burton, W.B., Liszt, H.S.: 1978, *Astrophys. J.* **225**, 815
Byrd, G.G.: 1976, *Astrophys. J.* **208**, 688
Byrd, G.G.: 1977, *Astrophys. J.* **218**, 86
Byrd, G.G.: 1978, *Astrophys. J.* **226**, 70
Casertano, S.: 1983, *Monthly Notices Roy. Astron. Soc.* **203**, 735
Cram, T.R., Roberts, M.S., Whitehurst, R.N.: 1980, *Astron. Astrophys. Suppl.* **40**, 215
Crovisier, J.: 1978, *Astron. Astrophys.* **70**, 43
Davies, R.D., Gottesman, S.T.: 1970, *Monthly Notices Roy. Astron. Soc.* **149**, 237
de Vaucouleurs, G.: 1978, *Astrophys. J.* **223**, 730
Emerson, D.T.: 1976, *Monthly Notices Roy. Astron. Soc.* **176**, 321
Habing, H.J., Miley, G.K., Young, E., Baud, B., Boggess, N., Clegg, P., Jong, T. de, Harris, S., Raimond, E., Rowan Robinson, M., Soifer, B.T.: 1984, *Astrophys. J. Letters* **218**, L59
Henderson, A.P.: 1979, *Astron. Astrophys.* **75**, 311
Henderson, A.P., Jackson, P.D., Kerr, F.J.: 1982, *Astrophys. J.* **263**, 116
Huchtmeier, W.K., Richter, O.-G.: 1984, *Astron. Astrophys.* (submitted)
Hunter, C., Toomre, A.: 1969, *Astrophys. J.* **155**, 747
Innanen, K.A., Kamper, K.W., Papp, K.A., Bergh, S. van den: 1982, *Astrophys. J.* **254**, 515
Kellman, S.A.: 1972, *Astrophys. J.* **175**, 353
Kerr, F.J.: 1957, *Astron. J.* **62**, 93
Kraan-Korteweg, R.C., Tammann, G.A.: 1979, *Astron. Nachr.* **300**, 181
Krumm, N., Shane, W.W.: 1982, *Astron. Astrophys.* **116**, 237
Kulkarni, S.R., Blitz, L., Heiles, C.: 1982, *Astrophys. J. Letters* **259**, L63
May, A., James, R.A.: 1984, *Monthly Notices Roy. Astron. Soc.* **206**, 691
Newton, K., Emerson, D.T.: 1977, *Monthly Notices Roy. Astron. Soc.* **181**, 573
Oort, J.H., Kerr, F.J., Westerhout, G.: 1958, *Monthly Notices Roy. Astron. Soc.* **118**, 379
Pellet, A., Astier, N., Viale, A., Courtès, G., Maucherat, A., Monnet, G., Simien, F.: 1978, *Astron. Astrophys. Suppl.* **31**, 439

Roberts, M.S.: 1966, *Astrophys. J.* **144**, 639
Roberts, M.S., Whitehurst, R.N.: 1975, *Astrophys. J.* **201**, 327
Roberts, M.S., Whitehurst, R.N., Cram. T.R.: 1978, in *Structure and Properties of Nearby Galaxies*, IAU *Symp.* No. 77, eds. E.M. Berkhuijsen and R. Wielebinski, Reidel, Dordrecht, p. 169
Rogstad, D.H., Lockhart, I.A., Wright, M.C.H.: 1974, *Astrophys. J.* **193**, 309
Rogstad, D.H., Wright, M.C.H., Lockhart, I.A.: 1976, *Astrophys. J.* **204**, 703
Rubin, V.C., Ford, W.K. Jr., Thonnard, N.: 1980, *Astrophys. J.* **238**, 471
Rubin, V.C., Ford, W.K. Jr., Thonnard, N., Burstein, D.: 1982, *Astrophys. J.* **261**, 439
Sancisi, R.: 1976, *Astron. Astrophys.* **53**, 159
Sancisi, R.: 1983, in *Internal Kinematics and Dynamics of Galaxies*, IAU *Symp.* No. 100, ed. E. Athanassoula, Reidel, Dordrecht, p. 55
Sancisi, R., Allen, R.J.: 1979, *Astron. Astrophys.* **74**, 73
Sandage, A., Humphreys, R.M.: 1980, *Astrophys. J. Letters* **236**, L1
Sawa, T., Sofue, Y.: 1982, *Publ. Astron. Soc. Japan* **34**, 189
Schwarz, U.J.: 1984, *Astron. Astrophys.* (submitted)
Shane, W.W.: 1975, in *La Dynamique des Galaxies Spiral*, Colloque International C.N.R.S. No. 241, ed. L. Weliachew, Editions du CNRS, Paris, p. 157
Shane, W.W.: 1978, in *Structure and Properties of Nearby Galaxies*, IAU *Symp.* No. 77, eds. E.M. Berkhuijsen and R. Wielebinski, Reidel, Dordrecht, p. 180
Shostak, G.S., Kruit, P.C. van der: 1984, *Astron. Astrophys.* **132**, 20
Sofue, Y., Kato, T.: 1981, *Publ. Astron. Soc. Japan* **33**, 449
Stark, A.A.: 1984, *Astrophys. J.* (submitted)
Toomre, A.: 1983, in *Internal Kinematics and Dynamics of Galaxies*, IAU *Symp.* No. 100, ed. E. Athanassoula, Reidel, Dordrecht, p. 177
Unwin, S.C.: 1980a, *Monthly Notices Roy. Astron. Soc.* **190**, 551
Unwin, S.C.: 1980b, *Monthly Notices Roy. Astron. Soc.* **192**, 243
Unwin, S.C.: 1983, *Monthly Notices Roy. Astron. Soc.* **205**, 773
van der Kruit, P.C.: 1981, *Astron. Astrophys.* **99**, 298
van der Kruit, P.C., Searle, L.: 1981a, *Astron. Astrophys.* **95**, 105
van der Kruit, P.C., Searle, L.: 1981b, *Astron. Astrophys.* **95**, 116
van der Kruit, P.C., Shostak, G.S.: 1982, *Astron. Astrophys.* **105**, 351
Visser, H.C.D.: 1980a, *Astron. Astrophys.* **88**, 149
Visser, H.C.D.: 1980b, *Astron. Astrophys.* **88**, 159
Westerhout, G.: 1957, *Bull. Astron. Inst. Netherlands* **13**, 201
Whitehurst, R.N., Roberts, M.S., Cram, T.R.: 1978, in *Structure and Properties of Nearby Galaxies*, IAU *Symp.* No. 77, eds. E.M. Berkhuijsen and R. Wielebinski, Reidel, Dordrecht, p. 175
Wright, M.C.H., Warner, P.J., Baldwin, J.E.: 1972, *Monthly Notices Roy. Astron. Soc.* **155**, 337